Cancer and Metastasis Reviews **24:** 441–467, 2005.

Review of Growth Inhibitory Peptide as a Biotherapeutic agent for tumor growth, adhesion, and metastasis*

M. Muehlemann[1,**,†], K.D. Miller[2], M. Dauphinee[3] and G.J. Mizejewski[4,‡]
[1]*Serometrix Biotechnology, Syracuse, New York;* [2]*Platelet Laboratory, University of Miami, Miami, Florida;*
[3]*Rumbaugh-Goodwin Cancer Research Institute, Plantation, Florida;* [4]*Wadsworth Ctr., Albany, N.Y. 12201*

Key words: alpha-fetoprotein, cell adhesion, peptides, receptors, platelets, extracellular matrix

Summary

This review surveys the biological activities of an alpha-fetoprotein (AFP) derived peptide termed the Growth Inhibitory Peptide (GIP), which is a synthetic 34 amino acid segment produced from the full length 590 amino acid AFP molecule. The GIP has been shown to be growth-suppressive in both fetal and tumor cells but not in adult terminally-differentiated cells. The mechanism of action of this peptide has not been fully elucidated; however, GIP is highly interactive at the plasma membrane surface in cellular events such as endocytosis, cell contact inhibition and cytoskeleton-induced cell shape changes. The GIP was shown to be growth-suppressive in nine human tumor types and to suppress the spread of tumor infiltrates and metastases in human and mouse mammary cancers. The AFP-derived peptide and its subfragments were also shown to inhibit tumor cell adhesion to extracellular matrix (ECM) proteins and to block platelet aggregation; thus it was expected that the GIP would inhibit cell spreading/migration and metastatic infiltration into host tissues such as lung and pancreas. It was further found that the cyclic versus linear configuration of GIP determined its biological and anti-cancer efficacy. Genbank amino acid sequence identities with a variety of integrin alpha/beta chain proteins supported the GIP's linkage to inhibition of tumor cell adhesion and platelet aggregation. The combined properties of tumor growth suppression, prevention of tumor cell-to-ECM adhesion, and inhibition of platelet aggregation indicate that tumor-to-platelet interactions present promising targets for GIP as an anti-metastatic agent. Finally, based on cholinergic studies, it was proposed that GIP could influence the enzymatic activity of membrane acetylcholinesterases during tumor growth and metastasis. It was concluded that the GIP derived from full-length AFP represents a growth inhibitory motif possessing instrinsic properties that allow it to interfere in cell surface events such as adhesion, migration, metastasis, and aggregation of tumor cells.

Introduction

Some of the most potent growth inhibitors known are peptide fragments derived from abundant plasma or extracellular matrix (ECM) proteins that themselves do not inhibit growth. The containment of a class of growth modulatory peptide segments within the structure of various circulating body proteins (their intrinsic peptides) appears to be a recurring theme in the field of signal transduction and growth regulation. A recent example was an occult (cryptic) binding site for tenascin on the fibronectin molecule [1]. The encrypted tenascin binding site was only detectable on proteolytic fibronectin fragments and when fibronectin was in an extended configuration. The fibrinogen receptor binding site on the platelet surface serves as another example of an encrypted binding site within a full-length protein [2].

Human alpha-fetoprotein (HAFP) is a tumor-associated fetal protein synthesized in fetal liver, yolk sac, and hepatomas [3–5]. HAFP has a molecular mass of 69 KDa and is largely alpha-helical, comprising three domains of nearly 200 amino acids (aa) each.

*Portions of the peptide data contained in this manuscript has been designated "Patent Pending".
**Corresponding author. E-mail: Muehlemann@illuminationtech.com
†Portions of the paper were presented at the 1st World Conference on Magic Bullets-Ehrlich, Sept. 9–11, 2004, Nuremberg, Germany.
‡Non-compensated scientific adviser.

This fetal protein also contains an encrypted peptide segment that is growth suppressive in its action [6]. Interestingly, in its native form, HAFP displays mostly growth-enhancing properties, regardless of whether the tissue is of fetal or cancer origin; thus, HAFP at physiological/pharmacological dose levels has been reported to enhance tumor growth [7–10]. Moreover, HAFP has been shown to possess pro-angiogenic properties that enhance neovascularization and growth in both fetal and tumor tissue [11,12]. Recent findings also indicate that HAFP can stimulate the expression of certain oncogenes (c-Fos, c-Jun, and n-Ras) which, in turn, enhances the proliferation of human hepatocellular carcinoma cells [13]. Human AFP, in vitro, has recently been shown to functionally impair dendritic cells inducing dysfunction and apoptosis of antigen processing cells (APCs). This latter report provided a mechanism by which hepatoma cells could escape immunological surveillance [14].

It was previously reported that a 34-amino acid peptide segment in the third domain of AFP can transiently bestow a growth suppressive property upon the full-length AFP molecule, in contradistinction to its growth enhancing properties [6]. A synthetic 34-mer peptide isolated from the third domain of HAFP encompasses a sequence stretch that normally lies buried in a molecular cleft in native HAFP (see Figure 1). This epitope cannot be detected using commercially available antisera to HAFP and requires an antibody distinct from monoclonal antibodies raised against full-length folded HAFP for its detection [15,16]. This encrypted peptide segment was initially discovered through its sequence similarity with members of the heat shock protein family (i.e., HSP-70) that are associated with (1) steroid receptor complex binding, and (2) transient protein folding/unfolding in the endoplasmic reticulum. Thus, exposure of the 34-mer exposed segment on HAFP might represent a folding intermediate form of the fetal protein (5). Indeed, this exposed peptide segment on the full-length HAFP molecule meets the described qualifications for being a folding intermediate protein marker as recently described [17]. An isolated synthetic peptide of this 34 mer amino acid segment has been termed the Growth Inhibitory Peptide (GIP; batch production #P149). It has now been demonstrated that the GIP was capable of growth suppression in a multitude of human tumors, both *in vitro* and *in vivo* [18]. In that latter report, it was proposed that the GIPs (including fragments) exert their anti-proliferative effects by serving as decoy ligands for G-coupled growth factor receptors. Thus, the mechanism of growth inhibition by the GIPs could be linked to a G-protein MAP kinase uncoupling mechanism in the course of signal transduction from the cell surface [18].

In a previous paper, it was demonstrated that the GIP was both an estrogen-and cytoskeleton-associated peptide capable of cellular uptake and cytoplasmic (perinuclear) localization [19]. It was observed that the GIPs were active at the cell surface plasma membrane which influenced cellular shape, form, immune agglutination, and peptide aggregation. Since cell shape and form are related to cytoskeletal events and microtubule-associated proteins, these cell-surface activities provided clues that the GIPs might be further capable of modulating cellular adhesion/attachment events. Furthermore, both native AFP and its derived GIP have been previously implicated with erthyrocyte agglutination and platelet aggregation as well as tumor cell adhesion to extracellular matrix proteins [5,20–22]. Therefore, the cell aggregation and adherence activities of GIP will be reviewed in light of its growth arrest properties in both human and murine cancers.

In the present review, several mammalian models of *in vivo* and *in vitro* oncogenic growth are summarized giving an overview of GIPs as growth inhibitors. Secondly, the results of various bioassays are surveyed which demonstrate that GIPs can inhibit and/or inactivate biological phenomena such as platelet aggregation, cell spreading, membrane enzyme activity, and cellular adherence involving integrins and tumor cells. Thirdly, a GenBank search was conducted to identify integrin, platelet, and ECM proteins that show amino acid sequence identity to short sequences from GIP [23]. Thus, this review focuses on the effects of GIP on neoplastic cell growth, and progression, adherence, and metastasis, in hopes of identifying GIP's molecular and cellular targets; this should aid in elucidating mechanisms of action of GIP regarding tumor growth inhibition and metastatic arrest.

Peptide synthesis, characterization, and properties

All peptides were synthesized by F-MOC chemistry using an Applied Biosystems 431A peptide synthesizer (Foster City, CA) as previously described [24–27] and purified on reverse phase high pressure liquid chromatography (HPCL). Control peptides included: a human albumin-derived peptide demonstrating sequences

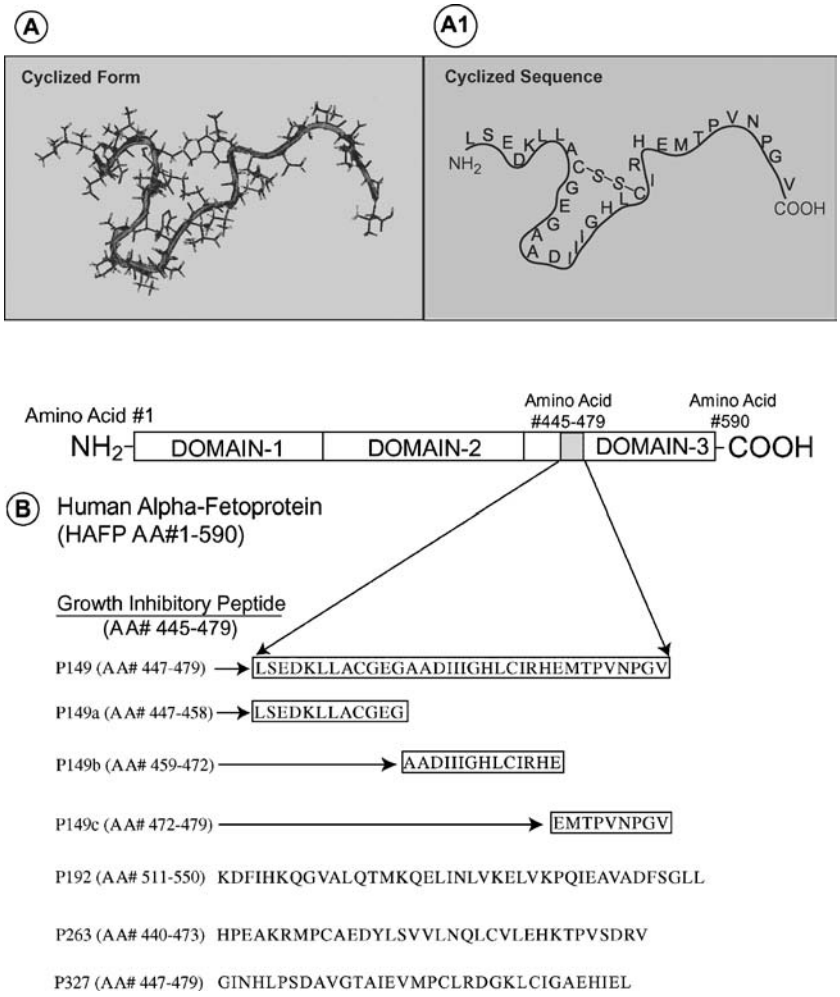

Figure 1. Panel-A: The cyclic version of, P149c the 34-mer Growth Inhibitory Peptide (GIP), is displayed in Panels A and A1 as a non-solvent computer model (See Ref. [48]). A1 shows the cyclized amino acid sequence. *Panel-B.* The three domains of human alpha-fetoprotein are shown in a bar configuration showing the 590 amino acid full-length protein. The telescoping segment displayed, from amino acids #445–477, is depicted in its single letter code amino acid sequence together with the three fragment constituents of P149 comprising P149a, P149b, and P149c. Control peptides P192, P263, and P327 constitute the bottom three peptides (see Ref. #6). The minimal energy computer non-solvent model of the cyclic peptide was kindly provided by Dr. Curt Brennerman, Dept. of Chemistry, Rensselaer Polytechnic Institute, Troy, NY.

which are located on a homologous amino acid stretch to GIP (P263), and a scrambled aa version of the P149 peptide termed P327 (Figure-1). Smaller peptide fragments of the 34-mer P149 (GIP) were also synthesized representing an amino terminal segment (P149a, 12 aa), a middle segment (P149b, 14 aa) and a carboxy terminal segment (P149c, 8 aa). In addition, Ovalbumin peptides were obtained from Sigma Chemical. Finally, an aspartic acid to aspargine (Asp $\rightarrow$ Asn) mutated peptide (P187) was employed as an aa- modified GIP for comparison of inhibitory activities. For other control peptides employed, see amino acid sequences in Reference #6.

The biochemical/biophysical studies of the 34 aa P149 revealed a peptide with a molecular mass of 3573 Da determined by electrospray ionization mass spectroscopy [24–26,28]. The far UV circular dichroism (CD) displayed a negative maximum at about 201 nm and indicated the presence of β-sheets/turns (45%) and other ordered structures in equal (45%) proportions, with the remaining structures composed of α-helices (10%) [26–28]. Both Fourier infrared spectroscopy

and GCG computer modeling software further confirmed the presence of a largely β-sheet structure for the peptide (Figure 1). A cyclic version of P149 was synthesized and computer modeled as displayed in Figure-1A together with the single-letter amino acid code sequences of GIP, its fragments, and the control peptides described above.

Comparison of peptide amino acid sequences

The aa sequences of all the GIP-peptides, P149, P149a, P149b and P149c were compared with protein sequences derived from the GenBank databases (Table 1) using the GCG (Wisconsin Program) FASTA sequence comparison software and criteria described in detail elsewhere [23,29]. Matches were found largely with proteins associated with integrins, the extracellular matrix (ECM) proteins, metalloproteinases, clotting factors, and adhesion proteins (Table 1). Matches were also found with integrin-associated ECM ligands such as collagen, laminin, fibronectin, and fibrinogen as well as with the integrin α/β chain proteins such as $\alpha_{11b}\beta_3$, $\alpha_1\beta_3$, and $\alpha_V\beta_1$ [30]. The integrins serve as receptors for ECM proteins and are known to participate in cell adhesion and migration (spreading) activities. Furthermore, GenBank matches were found with a number of blood clotting factors, which are also capable of interacting with the integrins. Finally, matches were also made with platelet-associated proteins, such as the Von Willebrand Factor and intergrin $\alpha_{11a}\beta_3$ which are involved in platelet activation, aggregation, and the action of metalloproteinases [31] Thus, P149 shows aa identity/similarity to integrins, platelets, ECM and blood clotting factors, all of which are involved in cell-to-cell and cell-to-ECM interactions.

Mouse Ascites mammary tumor

A mouse-induced mammary tumor 6WI-1 of adenoacanthoma (squamous) origin was obtained as described [32]. The growth suppression of the mammary ascites tumor by P149 and its fragments P149A, P149B and P149C, and control peptides, was determined in non-estrogen supplemented assays which measured tumor cell growth and ascites accumulation of 6WI-1 mammary tumors transplanted in NYLAR/nya mice [15, 18]. Tumor cell inocula included doses of 0.3, 1.0, and 3.0×10^6 cells which produced host mortality at 12–14 days being lethal in 100% of the animals. Following peptide dose titration studies [15] mice inoculated with 6WI-1 mammary cells were injected with a previously determined optimal dose of 1.0 μg peptide per day, or saline (controls) for 11 days. On day 12 following inoculation, the total accumulated ascites fluid volume and tumor cells in the peritoneal cavity of each animal were harvested and the total ascites cell count was determined [15].

Inoculation of mice at any of the three cell doses led to an increase in body weight from 25 g (day 0) to approximately 45 g by day 12, due to the accumulation of tumor cells and ascites fluid in the intraperitoneal cavity. An average cell count in the accumulated ascites fluid on day 12 was greater than 10^8 cells/ml with a total ascites volume of 20 mls in the body cavity. Tumor cell proliferation in this model has been reported to correlate with the volume of ascites fluid accumulated [15,18]. It was observed that the dose of 1 μg/day P149 for 11 days suppressed the tumor-associated body weight gain (significant, $p < 0.05$) at the two higher cell doses and totally suppressed body weight increase at the lowest cell dose (Figure 2). Mice in the totally suppressed group lived an additional 30 days until sacrificed. The P149 or its fragment P149C, but not P149A or P149B significantly suppressed the accumulation of both cells and ascites fluid volume at the highest cell dose (Figure 3; Table 2). Thus, the anti-tumor activity of P149 in the mouse mammary isograft was demonstrated by the peptide's suppression of approximately 45% of tumor cell proliferation and ascites fluid accumulation (3×10^6 inocula) as compared to the vehicle control (Figure 3). A scrambled peptide version of the GIP (P327) totally lacked anticancer activity in the mouse mammary isograft model (data not shown). As an alternative model of the 6WI-1 mammary tumor in adult mice, an inoculum of 1.0×10^6 tumor cells injected into 15-day old mouse pups provided a 6-day rather than a 12-day assay, and replicated the same tumor growth suppression by P149 (Table 2). Note that the P187 (Asp $\rightarrow$ Asn) mutated peptide showed slightly less growth inhibitory potency in the mouse pup model than did the original P149 peptide.

The peptide and non-peptide treatments in the 6WI-1 mouse mammary tumor studies were further compared by histopathological analysis of hematoxylin/eosin stained paraffin-blocked tissue sections (Table 3). It was readily apparent that the mammary tumor cells were highly invasive to many organs and tissues within the body cavity. Surprisingly, the liver, spleen, and kidney showed no apparent metastasis, invasion, or

Table 1. Amino acid sequence matching of growth inhibitory peptide (P149) with various extracellular matrix, clotting and adhesion-associated proteins.

																																	Percent (%) identity/ similarity	Percent (%) total
I. Extracellular Matrix Associated Proteins																																		
Hum AFP #445	L	S	E	D	K	L	L	A	C	G	E	G	A	A	D	I	I	I	G	H	L	C	I	R	H	E	M	T	P	V	N	P	G	V	G	100/100	100
Fragment P149					P149a											P149b												P149c								
Hum Laminin-A #032	L	S	E	I	K	L	L																												86/0	86
Hum α1 Coll IV #5		S	E	Q	R	L	P																				L	S	P	L	A	P	G	N		43/43	86
C. Eleg Coll α3			Q	R	K	L	L																				X	P	P	V	A	P	G	N		58/17	75
Hum Tenascin #93		T	I	T	K	L	I									I	F	Y	G	H	L	C	S	X	H										53/27	80
Hum Coll XIII #5								G	C	G	E	G	G	G	T												L	A	P	C	L	P	G	I		44/44	88
Rat Cerbrogly #520								A	C	G	R	G	L	L	E												A	A	P	X	X	P	G	V	G	53/13	66
Hum Coll-Sp #38								F	C	G	S	G	V	P	A												M	A	P	V	X	P	Q			50/14	64
Hum Elastin #400								P	C	G	S	A	S																P	F	P	P	G	V	G	50/29	79
C. Eleg LAP #330									C	G	D	G	A	A	D																					86/14	100
Hum Coll XVII										G	E	G	A	A	D	D	V	L	L	R	Y	C	T	K	R	E	I								44/28	72
Hum LAM-1 #88											E	G	S	S	N	L	V	X	R	H	M	V	I	K	W	Q	G	X	D	S	N	P	G	V	S	35/43	78
Xen Fib-α-C #80												S	G	T	T	I	I	V	E	H	L	I														40/45	85
Rat CSP-NG2 #55													Y	V	D	I	F	E	G	H	L															56/11	67
Hum Fibron #2070																						P	I	R	H	R	P	R	P	Y	P	P	N	V	G	50/14	64
Hum Coll-IV #90																											G	T	P	I	G	P	G	V		55/22	77
Hum Coll XIII #10																											G	T	P	I	G	P	G	V		55/22	77
Dros Laminin-A #660																											F	I	S	S	N	P	G	V	G	55/11	66
II. Matrix Metalloproteinase-Associated Proteins																																				
Xen BMP-Met #95	L	S	D	D	R	H	M																				I	V	P	V	G	P	G	V		53/33	86
Hum Lysyl #935				D	L	L	L	A	C	G	E	G	S																							80/10	90
Hum Prot-P3 #25													A	A	E	I	V	G	G	H	E															56/18	74
Rat Meprin #225													I	A	S	I	I	I	G	H	L	W	V													64/9	73
Rat G-Nexin #380																						C	I	R	H	N	P	T	G							63/13	74
Porcine MMP #398																											M	I	A	E	F	P	G	V	G	55/0	55
Rabbit Collag #45																											M	I	E	Y	F	P	G	V	G	55/11	66

(*Continued on next page.*)

Table 1. (*Continued.*)

																															Percent (%) identity/ similarity	Percent (%) total
III. Clotting-and Adhesion-Associated Proteins																																
Hum-VWF #1480	K	E	L	A	C	D	A	G	G	V	H	T	X	S	E	S	L	C	V	R	H	T	V	S	X	V	N				44/16	60
Chicken-TPA #470	G	L	L	X	C	G	T	G	A	A	C	T	V	S	G	H															60/7	67
Chicken Attach P. #2				R	C	G	E	G	A	R	G												V	G	V	G	G	G	G	V	G	47/18	65
Hum BF- #1270									I	S	Q	I	I	V	G	H	L														56/33	89
Hum BF-VIII #125									I	S	Q	I	I	V	G	H	L														56/33	89
Mus Compl – C5S #725										A	R	V	T	I	G	P	L	C	I	R											64/9	73
Mus Compl – C5D #725										A	R	V	T	I	G	P	L	C	I	R											64/9	73
Hum-TPA #4100												I	I	I	Y	H	L	C	I	I											78/0	78
Rat VLA-1 #755																		C	I	R	H	S	F	L	M	L	D				40/30	70
Hum α-IP10 #32																		C	I	S	I	S	N	Q	P	V	N	P	R	S	46/8	54
Hum PG-IIIA #180																		C	I	X	T	Q	L	G	P	V	N	P	A	L	50/41	91

Abbrevatives: AFP = Alpha-fetoprotein; Attach P = attachment (Adhesion) protein; BF = Blood Factor; BMP = bone morphogenetic protein (metalloproteinase); CSP = chondroitin sulfate proteoglycan Cerebrogly = cerebroglycan; Coll = collagen; Collag = collagenase; Collag – SF = sollagenase stimulatory factor; Compl = complement component; C. eleg = Caenorhabitis elegans; Dros = Drosophilia melanogaster; Fib = fibrinogen α-chain; Fibron = fibronectin; G-nexin = glial nexin protease; HUM = human; IP10 = interferon-α-induced chemokine; Lysyl = Lysyl hydroxylase; *Mus = mouse; MMP = matrix metalloprotease; Prot-P3 = proteinase protein (myeloblastin); PG-IIIa = platelet glycoprotein (fibrinogen receptor); TPA = tissue plasminogen activity; VLA-1 = integrin α1, (lamin & collagen receptor); VWF = von Willebrand's Factor; Xen = xenopus.

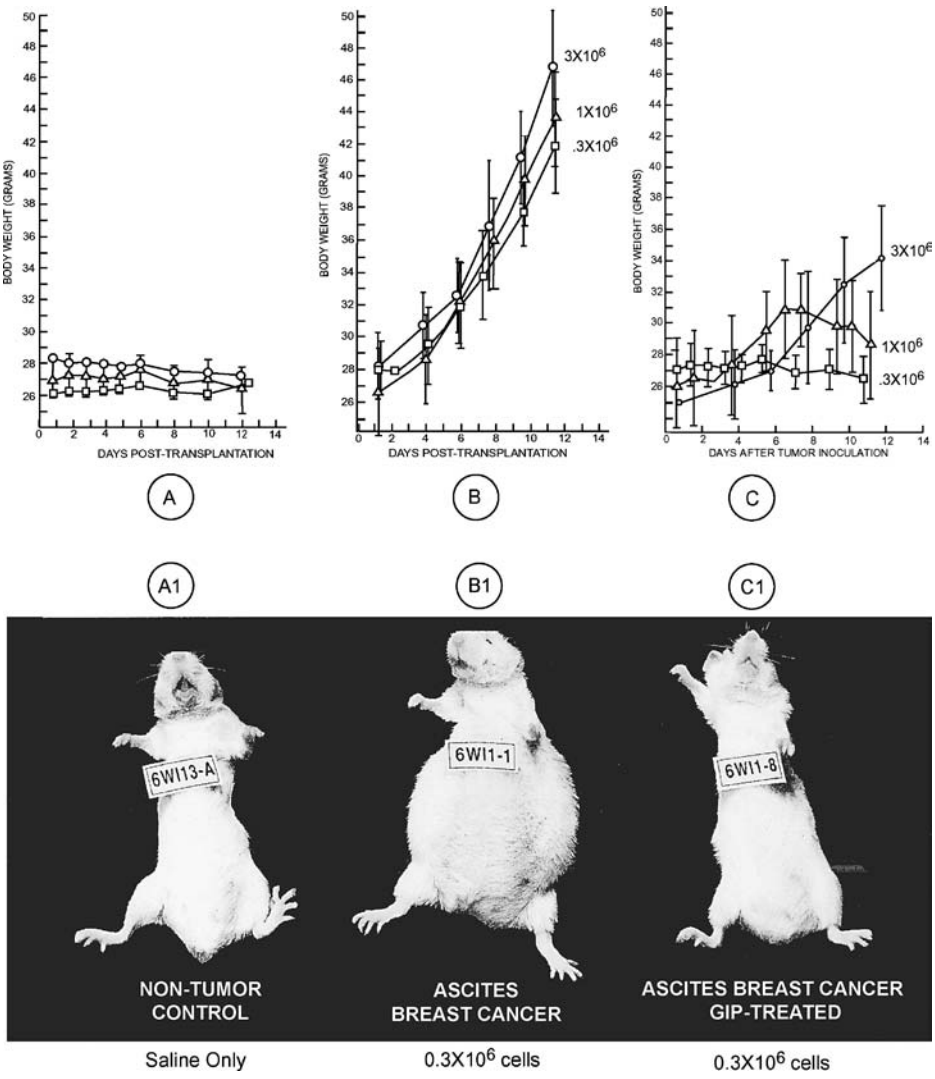

Figure 2. The serial transplantation in NYALAR mice of isograft 6WI-1 murine mammary tumor ascites cells is depicted at 3 different dose inocula. *A and A1*: a graph of three grouped body weight measurements over 11 days and a non-tumor treated animal are indicated, respectively; *B and B1:* a graph of three different dose dependent body weight increases over 11 days and an ascites-laden breast tumor inoculated mouse are indicated, respectively; *C and C1:* a graph of three different dose dependent body weight measurements and a GIP treated mouse at 0.3×10^6 cell inocula are indicated, respectively.

infiltration possibly due to their dense organ encapsulation. In contrast, the most extensive organ invasion and infiltration of tumor cells occurred in the retroperitoneal interface of the pancreas. The tumor was also selective for the parietal and pelvic peritoneum, especially the retroperitoneal serosa and fatty tissues surrounding the uterus, ovary, and kidney. Mammary tumor cells were identified in all treatment groups with a pattern of decreasing metastatic infiltration in the following order; non-peptide >scrambled peptide >GIP (Table 3). While large tumor masses were observed in the non-peptide treated group, and high-to-moderate tumor infiltrates were observed in the scrambled peptide-treated group, the GIP-treated groups displayed only minimal tumor infiltrates together with foci of lymphoid cells representing a host inflammatory response. Thus, the P149-treated mice could easily be distinguished from the saline and control peptide treated animals (Table 4).

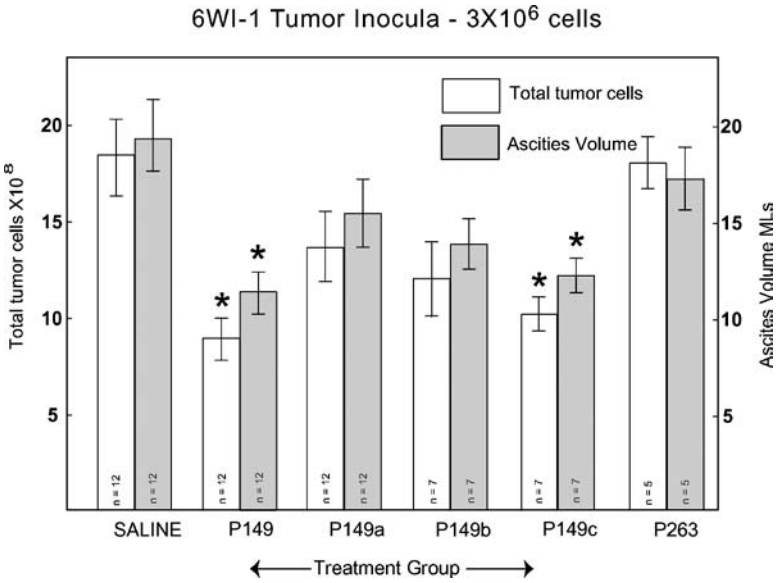

Figure 3. The growth suppressive activity of P149 linear peptide in the mouse mammary tumor isograft is demonstrated by the peptide's suppression of tumor cell proliferation and ascites fluid accumulation at a dose inoculum of 3×10^6 tumor cells. asterisk = significant difference at $P < 0.05$; P263 = control peptide; GIP = P149; GIP fragments = P149a, P149b, and P149c (see legend to Figure-1).

Effect of P149 on tumor cell lines

The initial report of an anticancer effect of P149 was reported in an estrogen-dependent contact-inhibition *in vitro* assay employing the human breast cancer MCF-7 cell line [6]. The P149 peptide suppressed the accumulation of tumor cell foci formed as a result of breast cancer cells which clump together due to loss of contact inhibition (Table 2). The suppression of estrogen-induced foci by P149 was extremely potent, displaying

Table 2. Comparison of the biological activities of growth inhibitory peptide (P149) and its three peptidic fragments are compared in various tumor and non-tumor *in vivo* and *in vitro* mammalian models.

	(%) Inhibition of activity						
Peptide segment/cell activity	P149	P149a	P149b	P149c	P263	P192	Ref.
1. 6WI-1							
A. Body weight	48	22	31	44	13	0	[15,18,30]
B. Cell proliferation	50	28	34	45	5	0	
C. Acites volume	42	21	26	39	10	0	
D. Pup ascites model	56 (50)	21	32	29	0	0	
E. Peptide combination	NA	P149a,b	44		0	0	
2. Kidney tumor growth	70	25	50	19	0	0	[30]
3. MCF-7 foci formation	68 (20)	33	31	45	0	0	[19,30]
4. Platelet agglutination	90	40	95	0	0	0	[20,21]
5. Uterine growth	39	28	22	42	0	0	[18,30]
a. Enzymatic fragments	NA	24	19	44	0	0	
6. Cell adhesion	65	ND	58	56	0	0	[5]
7. Estrogen fetoxicity	73	63	67	37	0	0	[28]

P149 = 34 mer Growth Inhibitory Peptide (GIP), ( ) parentheses indicates P187 activity; P149a = 12 mer aminoterminal of GIP; P149b = 14 mer midpiece of GIP; P149c = 8 mer carboxyterminal GIP; MCF-7 = human breast cancer glandular cells; Pup =16–18 day immature mouse. Peptide combination = P149a and P149b were injected together. P263 = homologous human albumin peptide; P192 = carboxy terminal peptide stretch from the third domain of HAFP. For % inhibition activities, see individual references.

Table 3. Histopathological findings of metastases of 6WI-1 mouse mammary tumor* in various organs of host animals injected with saline, scrambled control peptide (P327), or with growth inhibitory (P149) peptide.

Treatment group (N=5)	Gross findings	Liver	Spleen	Kidney	Pancreas	Uterus + ovary	Retro-peritoneal mesentery and fat	Abdominal muscle	Comment
1. Tumor + saline	Large tumor masses around intestine and colon	No infiltrate	No infiltrate	No infiltrate	Massive tumor infiltrate and necrosis	Tumor incased organ serosa	Extensive tumor infiltrate in fat tissue	Multiple tumor infiltrate	Extensive tumor encasement of organs and bowels
2. Tumor + scrambled peptide (P327)	Presence of tumor masses and foci	No infiltrate	No infiltrate	No infiltrate	Distinct presence of tumor infiltrate	Tumor encased organ serosa	Extensive tumor infiltrate and necrosis	Focal tumor infiltrate	Tumor infiltrate on organs and in mesentery especially fat tissue
3. Tumor + P149 peptide	Reduced tumor masses and foci	No infiltrate	No infiltrate	No infiltrate	Minimal tumor infiltrates; lymphoid response	Minimal tumor presence on organ serosa	Some tumor infiltrate; lymphoid response	Minimal tumor presence	Overall diminished tumor infiltrates throughout

*Mice received a tumor inoculuim of 1×10^6 cell via intraperitoneal injection. Peptides and saline vehicle were injected daily for 11 days with 0.1 cc volume delivered via a tuberculin syringe fitted with a 26 gauge needle. Tissue sections were examined by a New York State board-certified MD pathologist. Data derived from Reference #16. Tissue sections were stained with hematoxyln and eosin and examined using light microscopy. P237 = scrambled peptide (see text).

Table 4. The growth-suppressive effects of P149 (2-day vs 6-day screening results*) are displayed for multiple types of Human Tumor Cell Cultures*.

Tissue of origin human-derived	Cell line designation	Tissue tumor type	2-day assay		6-day assay	
			Conc. (molar)	(%) Growth inhibition	Conc. (molar)	(%) Growth inhibition
1. Colon	KM-12	AC	10^{-2}-10^{-1}	10–20	10^{-5}–10^{-7}	75
	HCC-299	AC	10^{-1}	20	10^{-5}, 10^{-7}	80
	Colo-205	AC	10^{-2}	10	10^{-5}	10
	HCT-116	AC	10^{-2}, 10^{-1}	15	10^{-5}–10^{-7}	75
2. Ovary	OVCAR-3	AC	10^{-2}	20	10^{-5}–10^{-7}	80
	SK-OV-3	AC	10^{-2}, 10^{-1}	10	10^{-5}–10^{-7}	60
	IGROV1	AC	10^{-1}	10	10^{-5}–10^{-7}	75
	OVCAR-4	AC	10^{-2}, 10^{-1}	20	10^{-5}–10^{-7}	85
3. Breast	MCF-7	AC	10^{-2}	20	10^{-5}–10^{-7}	80
	MDA-MD-231	AC	10^{-2}, 10^{-1}	25	10^{-7} only	80
	MDA-MD-435	AC	10^{-1}	20	10^{-5}–10^{-7}	70
	BT-549	AC	10^{-2}, 10^{-1}	15	10^{-6}–10^{-7}	25–40
	T-47D	AC	10^{-2}	10	10^{-5}	25
4. Prostate	PC-3	AC	10^{-1}	5	10^{-6}–10^{-7}	80
	DU-145	AC	10^{-1}	10	10^{-5}–10^{-7}	90
5. Non-small cell Lung	HOP-62	CA	10^{-2}, 10^{-1}	30	10^{-5}–10^{-7}	75
	NCI-H226	CA	10^{-2}	5	10^{-5}	5–10
	NCI-H460	CA	10^{-2}	30	10^{-5}–10^{-7}	80
6. Melanoma	UACC-62	Epithelial	10^{-2}, 10^{-1}	15–20	10^{-4}–10^{-7}	80
	SK-MeL-5	Squamous	10^{-2}	5	10^{-5}	10
	SK-MeL-2	Squamous	10^{-2}, 10^{-1}	20	10^{-5}–10^{-7}	50–75
	UACC-257	Squamous	10^{-2}	20	10^{-5}–10^{-7}	75-80
7. Central nervous system	SF-295	CA	10^{-2}, 10^{-1}	20–25	10^{-5}–10^{-7}	80
	SF-539	CA	10^{-2},	10	10^{-5}	15–20
	U-251	CA	10^{-2},	15	10^{-6}–10^{-7}	45
	SNB-75	CA	10^{-2}, 10^{-1}	10	10^{-6}–10^{-7}	50
8. Kidney	TK-10	Renal CA	10^{-2}, 10^{-1}	20	10^{-4}–10^{-7}	85
	RXF-393	Renal CA	10^{-1}	30	10^{-6}–10^{-7}	45–50
	ACHN	Renal CA	10^{-2}	20	10^{-7}–10^{-7}	80
	CAK-1	Renal CA	10^{-2}, 10^{-1}	15	10^{-5}–10^{-7}	50–75
9. White blood cell	K-562	Leukemia	10^{-2}, 10^{-1}	5	10^{-7}	45
	Molt-4	Leukemia	10^{-2}	5	NA	10–15
	CCRF-CEM	Leukemia	10^{-2}	5	10^{-5}	5–10

Cells were exposed to the peptide for two or six days, fixed, and stained with sulforhodamine-β. None of the cell lines were estrogen-dependent for growth.

AC = adenocarcinoma, CA = Carcinoma

*National Cancer Institute Therapeutics Screening Program, Bethesda, MD, used with permission. Data derived from Reference [15] and [18].

peak inhibitory doses at 10^{-10} to 10^{-12} M concentrations. Following that initial study, summary findings on P149 by the National Cancer Institute Therapeutics Drug Screening Program (Bethesda, MD) were disclosed (Table 5). These results detailed the *in vitro* studies of the GIP challenge against cell culture lines representing a variety of human cancers [18]. In a 2 day versus 6-day comparative proliferation assay (employing sulforhodamine staining), the P149 peptide appeared to be cytostatic (non-cytotoxic) against 38 of the 60 cancer cell lines, representing nine distinct cancer cell types which included prostate, breast, and ovarian cancers (Table 4). In subsequent reports, the effective use of the GIPs against various breast cancers was described in numerous studies involving breast cancer cells both *in vivo* and *in vitro* (Figure 4) (15). The P149 peptide (0.5 μg/day release pellets) also inhibited the *in vivo* growth of human breast cancer GI-101 cells, a non-estrogen-dependent, p53-responsive, tamoxifen-resistant ductal carcinoma transplanted as a xenograft in nude mice [33,34]. In these latter studies, time release pellets of P149 were administered for a 60-day

Table 5. Platelet-associated integrins alpha and beta subunits were compared to Growth Inhibitory Peptide (GIP) amino acid stretches.

Integrin subunits and original names	Cell/tissue distribution of integrins	ECM/cell binding ligand	GIP amino acid sequence stretch	P149 fragments (includes overlaps)	Platelet aggregation inhibition (%)	Tumor/tissue expression of integrins
$\alpha_2\beta_1$: VLA-2 (GP1a)	Epithelium Endothelium Leucocytes platelets	Coll, platelet	GEGAADIIIG; HLCIRHEMTPVNPG	P149a, b P149b, c	>90	Animal mammary carcinomas, human breast cancers
$\alpha_5\beta_1$: VLA-5 (GP1c)	Endothelium, hepatocytes, platelets	FBN, platelet	DIIIGHLC	P149b	>70	During growth and tumorigenesis
$\alpha_6\beta_1$: VLA-6	Most cells, epithelium, endothelium platelets	LAM, platelet	GEGAADIII; DIIGHLC	P149a, b P149b	>80	Breast, liver, lung carncinoma
$\alpha_{IIb}\beta_{3a}$: Major Platelet Receptor	Granulocytes, monocytes, megakaryocytes, platelets	FBN, FIB, VTN, VWF TSP	LSEDKLLACGEGAA; GHLCIRHE	P149 P149a P149b	>96 30–40 >90	Required for platelet aggregation
$\alpha_v\beta_3$: VTN receptor	Osteoclasts endothelium fibroblasts	FIB, VTN, FBN, FBG, COLL, VWF, TSP	EDKLLAC GHLCIRH	P149a, P149b	>70	Melanoma and angiogenesis

The GIP and Its Segments were then listed according to their platelet aggregation percent inhibition in lieu of their respective extracellular matrix ligands.

Abbreviations: Coll-collagen; FBG-fibrinogen; FBN-fibronectin; FIB-fibrin; LAM-laminin; TSP-thrombospondin; VTN-vitronectin; VWF-von Willebrand's factor; *-amino acid single letter code. Integrin data derived from References 5 and 30.

duration. In another study using a 30-day time-release pellet, P149 suppressed the *in vivo* growth of estrogen dependent growth of MCF-7 human breast cancer xenografts in nude mice using a pellet release rate of 0.25 μg peptide/day (Figure 4). In accompanying cell culture cytostatic assays, P149 suppressed by 50–80% the growth of four of five human breast cancer cell lines maintained in non-estrogen supplemented cell culture media, thus demonstrating an estrogen-independent mode of growth inhibition [15,18].

In the *in vivo* nude mouse xenograft studies, P149 was effective as a growth suppressing agent (70% inhibition) in the GI-101 breast tumor model even after withdrawal of peptide exposure. The GI-101 treated animals that had received the P149 pellet implant for 60 days, survived for 45 days after peptide depletion. At 105 days, the mice were sacrificed and the tumor volumes were recorded as an indicator of growth. When the remaining mice on P149 treatment were compared to sham controls, 3 of 4 surviving animals continued to display 40–50% tumor growth suppression. In another *in vivo* tumor study, nude mice were implanted with MDA-MB-231 (Non-estrogen receptor ER) breast tumor cells, and similarly treated with P149 time-release pellets. These tumors showed only minor growth suppression (30%) *in vivo* during administration of the 60-day GIP implants, resembling the results of the sulforhodamine *in vitro* assays, in which 30–40% growth suppression was seen. However, histopathological analysis following autopsy on day 105 (after GIP depletion) revealed that the tumor-bearing nude mice that received the P149 implants displayed metastases on an average of 1.5 nodules per lobe of the lung compared to 4.25 nodules/lobe in the lung of control tumor-bearing mice (5 mice/group).

In order to determine whether P149 was cytostatic or cytotoxic, an ATP-based assay was performed which measured the decrease in cytosolic ATP during drug (peptide) treatment. This ATP luminescence assay has long been employed to distinguish between cytostatic versus cytotoxic chemotherapeutic sensitivity of drugs [35–37]. Since cells maintain their ATP concentrations nearly constant under physiological conditions, metabolic disturbances (i.e., injection of toxic agents) will result in a gradual decrease of the total amount of cellular ATP. In contrast, cell death is accompanied by a rapid and complete

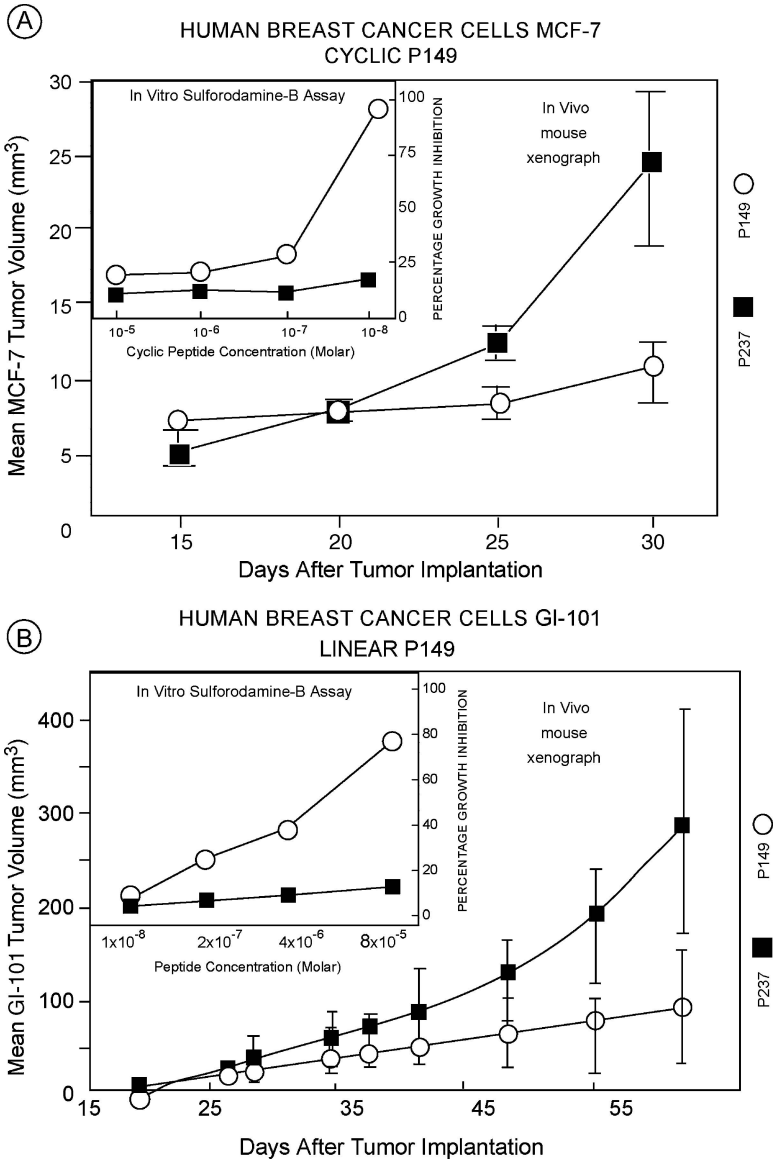

Figure 4. Two different human breast cancer cell lines were assayed both *in vivo* and *in vitro* using the cyclic and linear versions of P149 peptides. *Panels* A: An *in vivo* study of cyclic P149 was performed using E2-dependent MCF-7 xenograft in nude mice. The mice received both estradial and P149 peptide time release pellets over 30 days. The *inset* in panel-A depicts the same peptide studied *in vitro* using sulforhodamine-B growth inhibition assays. *Panels B* An *in vivo* study employing P149 linear peptide was conducted in nude mice implanted with estrogen-independent GI-101 human ductal cancer cells using P149 peptide time release pellets over 60 days. The inset in panel-B shows the same peptide studied *in vitro* using sulforhodamine-B growth inhibitors assays. Note that even though the *in vivo* assays showed similar curves, the *in vitro* dose response of the linear peptide required three log dose increases in concentration to produce a similar effect to the cyclic peptide.

loss of ATP. After incubation of the cell cultures for 6 days, cytosolic ATP was extracted, stabilized, and quantitated from a standard curve produced from Berthold LB-96P luminometer readings using a luciferin-luciferase counting reagent. The ATP-bioluminescence assay of both MCF-7 cells and GI-101 cells exhibited a cytosolic decrease of ATP in P149 treated mice compared to both peptide-treated and control peptide treated cells. The results displaying the difference in cytosolic ATP over a 6-day period were

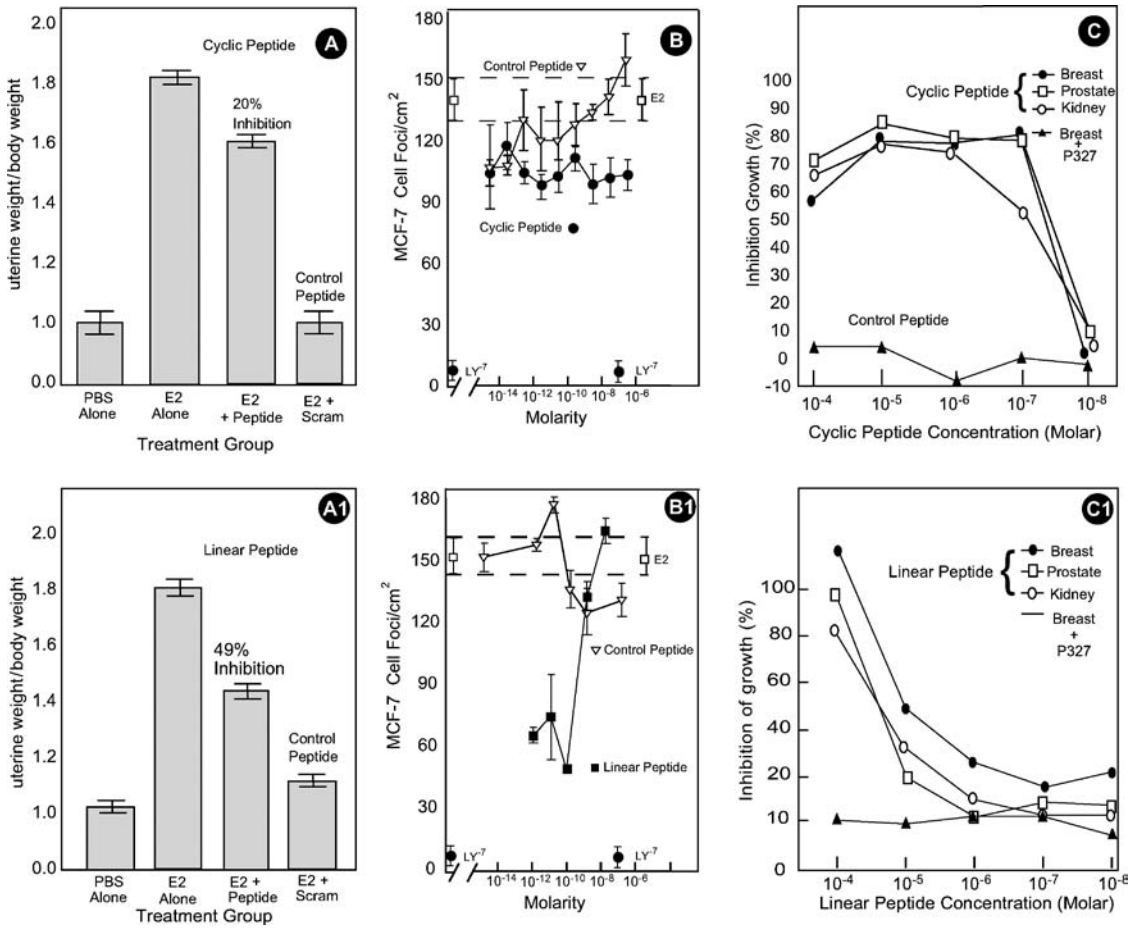

Figure 5. The growth suppressive activities of the oligomeric forms of P149, cyclic versus linear, are depicted in various *in vitro* and *in vivo* models. Biological activity was determined by three growth-associated bioassays, namely; Panel-A and A1) an immature rodent uterine bioassay; Panel-B and B1) an *in vitro* MCF-7 foci assay, and Panel-C and C1) an *in vitro* tumor cell cytostatic assessment. Results show that the linear peptide was highly dose effective in the mouse uterine assay (A1), and the MCF-7 foci-assay (B1), but not the *in vitro* cytostatic-assay (C1); while the cyclic configuration performed poorly in the uterine (A) and foci-assays (B), but extremely well in the *in vitro* cytostatic assays (C). See text for details. Scrambled peptide = P327.

deemed consistent with the presence of a cytostatic (rather than cytotoxic) mode of growth inhibition at peptide doses of 10^{-8} to 10^{-12} M, (see Figure 4, Panel insets).

The oligomeric forms of GIP used in the cytostatic assays also showed differences in their dose effects. The cyclic form of GIP (Fig. 1) is a disulfide-bridged cyclic monomer in solution, whereas GIP in the linear configuration is known to exist as a trimer [24–26]. Using three different human cancer cell lines (breast, prostate, kidney), it was demonstrated that the monomeric cyclic form of the peptide produced 80–90% growth inhibition over a range of 10^{-5} to 10^{-7} M, as assessed by the sulforhodamine 6-day assay (Figures 4 and 5). In comparison, the same three cancer cell lines produced growth inhibition at only 10^{-4} M and 10^{-5} M, which rapidly declined thereafter when the linear peptide was utilized. The cyclic monomeric form is depicted in Figure 1 and the linear form was described in detail in Ref. [19]. The linear peptide is known to be in the trimer/hexamer configuration [24], and eventually a higher-order polymer state may be attained after prolonged storage of the phosphate-buffered saline (PBS)-solubilized peptide. It is also apparent in Figure 5(b), that the cyclic versus the linear version of P149 produced different dose

responses when applied to the E2-dependent MCF-7 cell foci assay showing an inhibitory effect with low concentrations of linear but not cyclic peptide [6]. A third example (Figure 5(a)) is the E2-activated immature mouse uterine growth assay, in which the cyclic peptide was only marginally growth inhibitory, while the linear peptide achieved nearly 60% inhibition [18]. It can be deduced from these data that the oligomeric form of the GIP will determine the most effective growth inhibitory concentrations for the peptide in a given dose-dependent assay.

It was next deemed necessary to determine whether the various segments of P149 exhibited tumor suppressive capabilities similar to those of the 34-mer GIP. The linear GIP was used since the fragments did not form cyclic compounds for comparison. In a study employing a human kidney tumor cell line, it was further demonstrated that linear P149 and its linear fragments (P149 a,b,c) demonstrated individual growth inhibitory capabilities. For example, while the 34-mer P149 displayed nearly 80% growth inhibition of this tumor at 5×10^{-4} M, fragments P149b, P149a and P149c showed lesser potencies, of 50, 25, and 20%, respectively (Table 2). As in previous animal models, the fragments of P149 displayed less biological activity than did the entire 34-mer peptide [18,19]. It was obvious that the inhibitory potency of the whole P149 was not the sum of its peptidic segments.

Cell adhesion assays

Human AFP possesses short amino acid stretches that have sequence identity with a variety of ECM Proteins [5,18,30]. Therefore, P149 was subjected to cell adhesion studies involving some of the principal ECM proteins. The various ECM proteins were adsorbed to microtiter plates and screened for their abilities to serve as substrata for enhanced breast tumor cell adhesion compared to non-ECM matrix microtiter plates. Following crystal violet staining, the ECM proteins differed in their abilities to serve as attachment surfaces for two breast cancer cell types, the human MCF-7 and the murine 6WI-1 lines (Figure 6A). The mouse mammary 6WI-1 tumor cell attachment ranged from 20 to 60% for all ECM protein matrices, with laminin demonstrating the greatest adhesion capability (60%). Fibrinogen ranked second as an adhesion protein, with fibronectin and the collagens closely following. Non-protein attachment agents such as gelatin, chondroitin sulfate, and poly-lysine exhibited somewhat reduced cellular adhesion (20–40%) relative to the ECM proteins. In the studies using the MCF-7 cells, most of the ECM proteins were capable of supporting tumor cell adhesion to some extent. Cell adhesion in the MCF-7 cells ranged from 20 to 58%, with fibronectin achieving the highest proportion of attachment. While laminin supported little MCF-7 cell attachment (<5%), collagens I and IV displayed from 30 and 50%, and with fibrinogen displayed 20%. Interestingly, P149 (10μg/ml) itself was capable of supporting 20 to 25% cellular adhesion with both tumor cell types. The GIP was a slightly weaker agent of tumor cell attachment than was gelatin, chondroitin sulfate, and poly-lysine.

The adhesion of MCF-7 and 6WI-1 cells either in the presence of peptide or in peptide-free medium was then assayed on ECM-coated microtiter plates, with 3μg of soluble P149/well used as a competitive inhibitor (Figure 6(b)). The P149 was added to the wells immediately after the cells were dispensed and the mixture was then incubated as described [38]. The P149 peptide was capable of inhibition of cell adhesion to most of the ECM proteins in both tumor cell lines (Figure 6). Inhibition of mouse and human tumor cell adhesion was roughly equivalent on the plates with collagen IV, fibrinogen, fibronectin, and thrombospondin; however, cell adhesion inhibition was significantly different for laminin, collagen-I, and vitronectin when the two tumor types were compared. Human MCF-7 cells, in the presence of P149 displayed substantial inhibition to vitronectin-induced adhesion while mouse tumor cells failed to respond. Likewise, mouse 6WI-1 cells demonstrated peptide inhibition of laminin adhesion, whereas MCF-7 cells failed to adhere to laminin. Overall, the P149 peptide, in the presence of tumor cells, was found to competitively inhibit MCF-7 and 6WI-1 cell attachment by 40–50%. Thus, P149 was found capable of eliciting various degrees of adhesion inhibitions, dependent on the type of ECM protein coating the wall of the microtiter plate and also the tumor cell type involved (monolayer vs. ascites-derived). It was also found that an albumin 34-mer peptide control (P263) was not capable of inhibiting tumor cell adhesion, and that rabbit anti-P149 peptide antibodies completely blocked the adhesion inhibition effect (not shown). Also, the addition of high Ca^{2+} levels to the culture medium failed to influence either ECM adhesion to the microliter plates or the peptide inhibition of tumor cell adhesion to the ECM matrices.

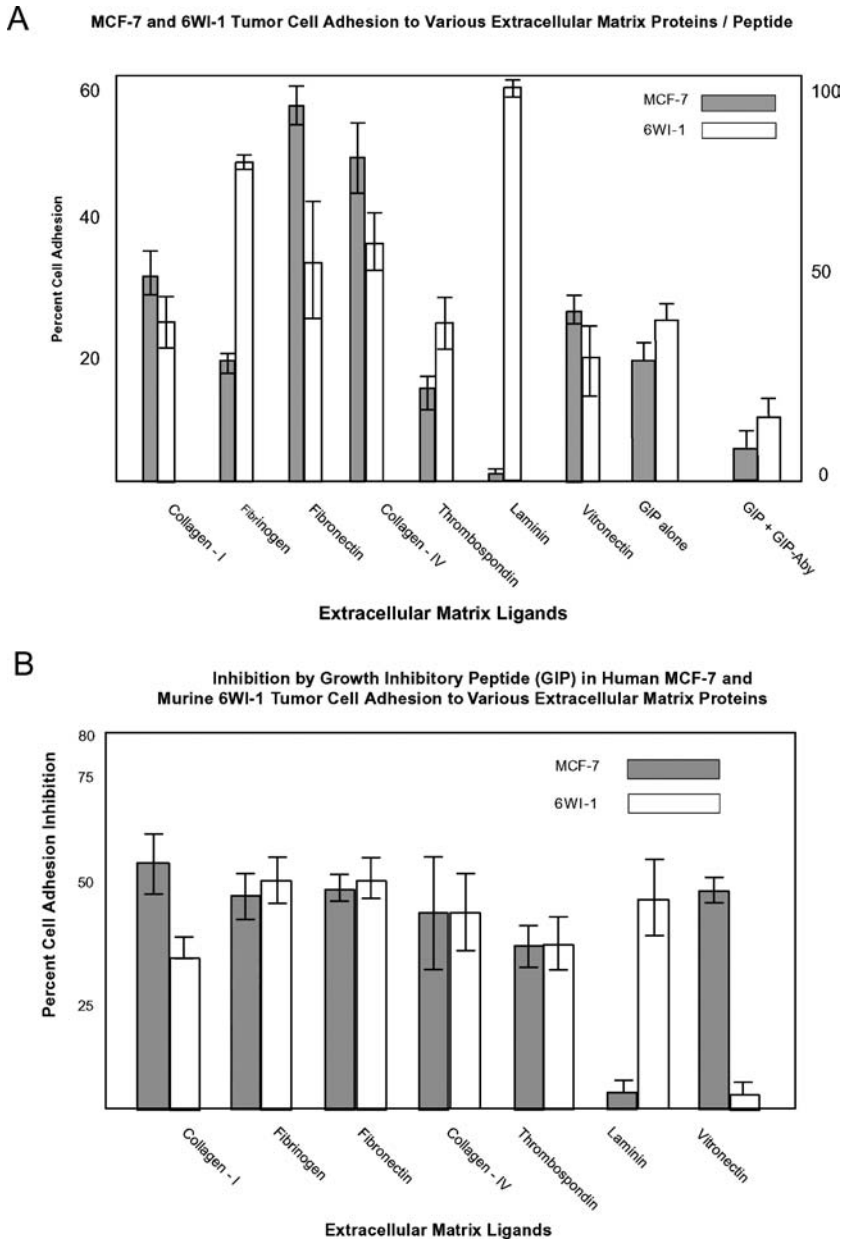

Figure 6. Panel A: The cellular adhesion of cancer cells to extra-cellular matrix (ECM) proteins and GIP is displayed for both human MCF-7 breast cancer cells and for murine 6WI-1 ascites-adapted-mammary tumor cells. The cellular adhesion assay was performed in 96-well microtiter plates and the wells were pre-coated with 100 microliters of each of the above-mentioned ECM proteins for 24 hours, tumor cells added, and the plates were then incubated at 37°C. While 6WI-1 cells usually required only 2–4 hours incubation for adhesion, MCF-7 cells required 24 hours for attachment following cell trypsinization and plating. The plates were washed twice with Hank's Saline, fixed in 0.5 mL of 37% formaldehyde, stained with crystal violet and read at 570 mm on a microplate reader. Note that GIP can provide a matrix attachment surface for tumor cell adhesion and that rabbit antibodies to GIP decreases tumor cell adhesion.
Panel-B: The P149 inhibition of cellular adhesion of cancer cells to extra-cellular matrix (ECM) proteins plus GIP is displayed for both human MCF-7 breast cancer cells and murine 6WI-1 ascites mammary tumor cells. The cellular adhesion assay was performed in 96-well microtiter plates and the wells were pre-coated with 100 microliters of each of the above-mentioned ECM proteins for 24 hours as previously determined. After adding tumor cells, the plates were then incubated at 37°C for various time intervals as above (Panel-A). The plates were washed twice with Hank's Saline, fixed in 0.5 mL of 37% formaldehyde, stained with crystal violet and read at 570 mm on a microplate reader.

It was also demonstrated that P149 subfragment possessed anti-cell adhesion capabilities (Table 2).

Tumor cell migration and spreading

The P149 treated, untreated and ovalbumin peptide-coated coverslips were placed in individual 24-well microtiter plates for assessment of MCF-7 cell spreading and migration [38,39]. Results of the cell spreading/migration studies revealed that the P149 coated surfaces caused inhibition of cell spreading over a concentration range, which peaked at 10 μg/ml (Figure 7). The cells, unable to migrate, and spread, displayed distorted morphology such as star-shaped configurations, cytoplasmic spiking, surface spiny spheres, and extended cytoplasmic processes, as well as low cell viability. These data support the findings from the cell adhesion studies described above and re-affirm that P149 is implicated in cell surface activities and cell-to-ECM interactions related to integrin involvement possibly with basement membranes, interstitial surfaces, and connective tissues.

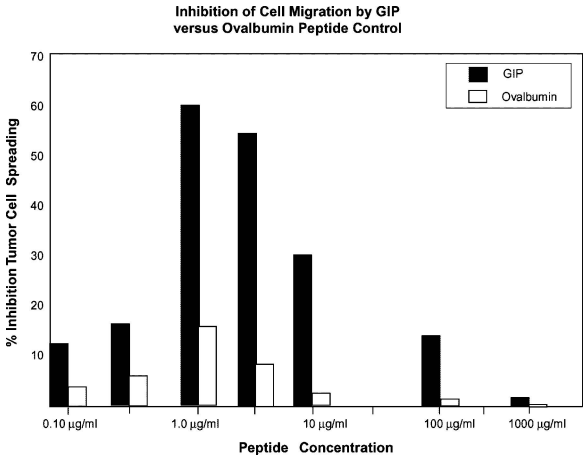

Figure 7. MCF-7 breast cancer cells were cultured for 3–4 days (80% confluence) in order to study tumor cell attachment, migration and spreading. The MCF-7 cells grown to confluence were harvested using trypsin digestion; the separated cells were resuspended in DC5. One day prior to cell seeding, glass coverslips were incubated in P149 or ovalbumin peptide concentrations extending from 0.1 μg/ml to 1000 μg/ml. MCF-7 tumor cells were seeded at 3×10^5 cells/well and incubated for 24 hours on the coverslips. Using the Crystal Violet stain, 100 microliters of 37% formaldehyde was then added to each well for 5 minutes for cell fixation onto the plates, the wells were washed twice, and 200 microliters of Crystal Violet staining solution was added, washed and dried. The coverslips were examined under light microscopy (see text).

Most cells (including cancer cells) need to attach and subsequently spread on the ECM substrate for proper growth, function, and survival [40]. In tissue formation, cells attach to one another and to the meshwork of the ECM, in a process mediated by the family of integrin proteins. Normal epithelial cells often undergo inappropriate apoptosis when deprived of ECM attachment [41]. Cell growth and survival on substratum (matrix) attachment has been termed anchorage dependence [41,42]. In cell culture, this linkage occurs at specialized membrane structures referred to as focal adhesions, consisting of clusters of integrins that are firmly bound to the ECM interface [42,43]. More loosely bound focal contacts, characteristic of epithelial tissues, probably permit some flexibility and cell movement. These integrin clusters serve as attachment points for intracellular actin stress fibers on the cytoplasmic surface of the plasma cell membrane, thus influencing cell shape. It is also at such focal points (see above) that integrins can trigger signaling pathways that cross-talk with growth-factor, cytokine, and kinase pathways [44], the latter include the focal adhesion kinase (FAK) [45,46]. Such cascade interactions are reportedly linked to G-proteins and the tyrosine kinases of the *src* family. It has also been reported that tissue-derived cells that spread and then flatten appear to thrive, whereas cells that retain an overall rounded form fail to survive [43]. Depending on the integrin heterodimer involved, differing anti-apoptotic effects of cell spreading have been delineated and described [45,47,48]. These reports revealed that following the ECM determination of cell morphology, cell shape was a major factor in determining subsequent cell growth and survival. It has been reported in a previous study that P149 can alter both cell shape and form [19]. Thus, it appears that therapeutic intervention at the integrin-ECM interface (as P149 might perform) could provide a means of altering the cell signals responsible for the balance between cell death and cell survival.

Platelet aggregation (*in vitro*)

The GIPs were assayed for human platelet aggregation through measurement of their degree of light transmission with an aggregometer, using stirred human platelet suspensions in a reaction vessel [49,50]. Following the addition of agonist, activation of platelet aggregation proceeds in a multi-step process. As a first step, activators cause the platelets to change shape

inducing a slight decrease in light transmission. As aggregation proceeds, the platelets form increasingly larger clumps, leading to an increase in light transmission throughout the reaction vessel. The light transmission increases progressively as aggregation begins, and reaches a plateau when aggregation is maximal. The aggregation profile can be further divided into two phases: (a) primary aggregation, which is an immediate and reversible process; and (b) secondary aggregation, which is irreversible and is associated with granule release and thromboxane generation. The secondary aggregation phase, depending on the agonist, liberates arachidonate for thromboxane A_2 formation [50,51]. In the data below, P149 is shown to be capable of affecting all phases of platelet aggregation.

The platelet cytoskeletal-induced response to activation first produces a shape change from the discoid to the sphenical form which initiates the aggregation step, in which increasingly larger clumps are formed. As discussed above, the GIP has been previously shown to influence cytoskeletal activation leading to changes in both cell shape and form [19]. The shape change also induces expression of pro-coagulant and phospholipid receptor activities; these in turn induce inositol phospholipids to increase the turnover of phosphatidic acid [49]. In the event of a blood vessel rupture, for example, the release of agonists from secreted granules activates blood platelets to manifest the discoid-to-spheroid shape change, and to send out long filopodial extensions from the platelet cytoplasm. The agonists further cause (1) the centralization of platelet cytoplasmic organelles, (2) release of platelet granules, and (3) formation of a "hemostatic plug" to prevent further blood loss from the blood vessel rupture [49].

Platelet activators, such as adenosine diphosphate (ADP), induce shape changes just prior to the primary and secondary aggregation [52]. The GIP was capable of inhibiting the shape change in the platelet response (Figure 8). Platelet shape and form are dictated by the submembraneous plasma membrane cytoskeleton, composed mainly of actin/myosin filaments [53]. ADP induces the change in cell shape through a cytoskeletal (mechanical) force-driven redistribution of organelles within the platelet cytoplasm. In a previous report, P149-interaction with the plasma membrane cytoskeleton and microtubule polymerization has been documented in several models, including elements of α-tubulin and actin filaments [19]. The polymerization of actin causes actin filament formation, which in turn induces a conformational change in the platelet cell-surface fibrinogen receptor ($\alpha_{11b}\beta_3$). The fibrinogen binding domain is concealed on the surface of resting platelets, and addition of platelet activators (i.e. ADP, arachidonic acid (AA), Collagen) exposes such sites [52]. As stated earlier, a conformational change in the HAFP molecule also serves to expose the hidden GIP site in a similar manner [15].

The ability of P149 and its fragments were next individually examined for their abilities to inhibit platelet aggregation in an assay using fresh citrated human platelet-rich plasma (PRP) from healthy volunteers. The peptides were dissolved in 0.15 M NaCl containing 2.5×10^6 platelets/ml. The various platelet agonists used as activating agents were ADP at 3μM final concentration, collagen at 2 to 5 μg/ml PRP, AA at 300 μM and epinephrine (Epi) at 5 μM. When concentrations of ADP were added to the platelet-rich plasma, the two phases of aggregation fuse to give a large aggregation response that does not reverse. P149 was able to dramatically inhibit the secondary ADP-induced aggregation response. The P149 peptide (100–300 μg/PRP) inhibited ADP induced platelet aggregation by 90–95%; while at 10 μg P149, inhibition did not occur (Figure 8; Table 6). It was shown that the P149b midpiece peptide, containing a von Willebrand Factor sequence identity, also inhibited ADP-induced aggregation, in a reaction with an initial slight delay, followed by a 80–90% inhibition that was not as dramatic as P149 itself. Further characterization of the ADP-induced inhibition by P149 included a titratable decline in surface-expressed CD62 (P-selectin) fluorescent staining of ADP-activated platelets assayed by flow cytometry. The P-selectin protein is a 140 KDA platelet surface marker induced by thrombin and is expressed on platelets, endothelial cells, and megakaryocytes [52]. Platelet selectin mediates platelet and neutrophil adhesion to endothelial cells during the adherent and rolling stages of neutrophil migration along the inner vascular endothelial wall. It is of interest that GIP also has been shown to inhibit agonist-induced thrombin and tissue-factor responses in immature rats [6,19] (Table 3).

When collagen was used as an activator of platelet aggregation, P149 (100μg) was capable of inhibiting >90% of the collagen-induced secondary aggregation response (Table 6). However, no significant inhibition was observed with P149c for both collagen and ADP-activated platelets. Both P149a and P149b were capable of inhibiting by >70–80% the platelet aggregation induced by ADP and collagen. Thus, the latter fragments

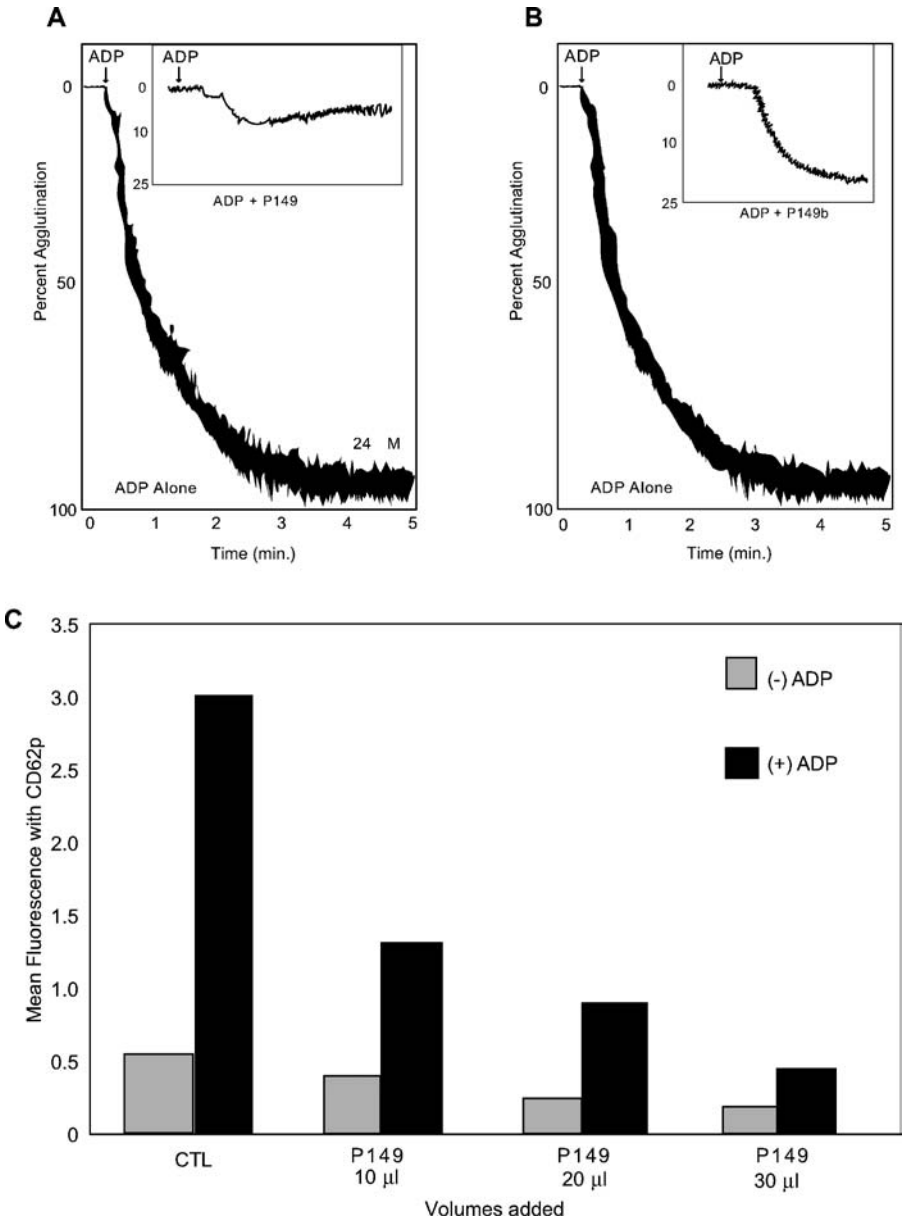

Figure 8. The platelet aggregation study is depicted in treatments involving 0.5 ml of normal human platelet-rich plasma (PRP) with varying amounts of P149 or P149b using 2.5×10^6 platelets per reaction vessel. After 2 minutes of stirring to obtain temperature equilibrium at 37°C, adenosine diphosphate (ADP) was added to the reaction vessel A: ADP incubated with P149 inhibited all phases of the platelet aggregation; B: P149b inhibited 70% of platelet aggregation; C: platelet aggregation by P149 as measured by CD62P (P-selectin) fluorescence quenching by means of flow cytometry.

of P149 (P149 a,b) were capable of inhibiting platelet aggregation to a lesser extent than intact P149; however, the P149 fragment aggregation inhibitions were significant considering that P149c was totally inactive (Tables 2 and 6).

The third type of platelet activation was induced by AA whose aggregation reaction commenced immediately after addition of AA to the reaction vessel (Table 7). Moreover, addition of P149 or P149b (shown in Figure 9) resulted in complete aggregation

Table 6. A summary of percent inhibition of human platelet secondary aggregation induced by various activation agents is listed for Alpha-fetoprotein Derived Growth Inhibitory Peptides and control peptides.

	Inhibition (%) of platelet aggregation			
Inhibitory peptide	Adenosine diphosphate (ADP)	Archaridonic acid (AA)	Collagen (COL)	Epinephine (EPI)
P149 (34-mer)		100	>95	No effect
P149a (12-mer)	30–40	10–20	75	No effect
P149b (15-mer)	95–98	100	70–80	No effect
P149c (8-mer)	No effect	No effect	No effect	No effect
α_2 AP (pos.control)	85–90	100	90	No effect
P263 (Homology control)	80–90	Shape change only	60–80	No effect
P192 (neg. control)	No effect	No effect	No effect	No effect
Ristocetin (positive control)	100	100	100	100

ADP = 2.5 μM; AA = 0.3 mM; Collagen = 2 μg/ml; EPI = epinephrine

P149 peptides were effective inhibitors in separate activation (agonist) experiments. P149 = Growth Inhibitory Peptide; P149a, P149b, P149c = Fragment of Growth Inhibitory peptide (see Table 1). α_2AP = peptide sequence from α_2-antiplasma; P263 = human albumin peptide segment; P192 = peptide sequence from HAFP molecule carboxy terminal end of P149. Ristocetin-a bacterial protein employed as a positive control for platelet aggregation inhibition.

Table 7. Biological/Biochemical activities of Growth Inhibitory Peptide (P149) exhibiting cross-reactivity in various species, organs, and tissues.

Biological/Biochemistry activity	Organism, class or species	Organ and/or tissue	Effect or action	Reference citation
1. Estrogen induced organ growth	Rats, mice	Uterus	Growth suppression	[6,18,19,25,26,]
2. Cell-to-cell contact inhibition	Human (MCF-7)	Breast cancer	Suppression of cell foci	[18,19]
3. Esterase enzyme activity	Rat	Uterus	Suppresses esterase activity	[6]
4. Fetal growth retardation	Chick, mouse	Whole body	Induces retardation	[28]
5. Amphibian metamorphosis	Frog	Tail fin epidermis, connective tissue	Inhibits differentiation	[81]
6. Insect ecdysis	Brineshrimp	Shell hatching	Inhibition	[18]
7. Insulin fetotoxity	Chick fetus	Musculo-skeletal system	Inhibition	[28]
8. Estrogen fetotoxicity	Mouse fetus	Whole body	Inhibition	[28]
9. Aromatase enzyme activity	Rat	Liver microsomes	Suppresses aromatase acivity	[19]
10. Platelet aggregation	human	vascular platelets	Inhibits aggregation	[18,19]
11. Cancer growth	Mouse, rat human	Breast cancer cells	Growth inhibition	[18,19]
12. Fetal malformation	Chick fetus	Whole body	Birth defect suppression	[18,28]
13. Acetylcholinesterase (Ache) activity	Torpedo eel	Soluble tissue extracts	Inhibits soluble Ache activity	[18,19]
14. Estrogen receptor-α binding	Human	Recombinant receptor	Binding to α-ER receptor	[15,19]
15. Cortisone induced Splenic Growth	Mouse pup	Whole organ	Growth suppression	[82a,82b]
16. Estradiol binidng	Human	Purified peptide	Binding to GIP (P149b)	[15,19]
17. Litter size	Mouse newborn	Whole body	Inhibits reduced litter size	[19,28]
18. Ovarian HCG-growth stimulation	Mouse pup	Whole body	Suppresses growth of ovary	[19,82a,82b]
19. Tumor ascites fluid	Adult mouse	Body cavity fluid	Suppression of fluid accumulation	[15,18]
20. Red blood cell (ABO system)	Human	Erythrocytes	Blocks Hemoagglutination	[19]

P149 = 34 mer GIP; P149b = 13-mer midpiece GIP, ABO = red blood cell antigens; ER = estrogen receptor.

Ref. #82a = Mizejewski, G. J. Growth inhibitory peptide, United States Patent 5, 674, 842, U.S. Patent Office Filing US00567 484A, Oct. 7, 1997.

Ref. #82b – 82b Mizejewski, G. J. Methods of using growth inhibitory peptides. United States Patent 5, 707, 963, U.S. Patent Office Filing US005707, 963A, Jan. 13, 1998.

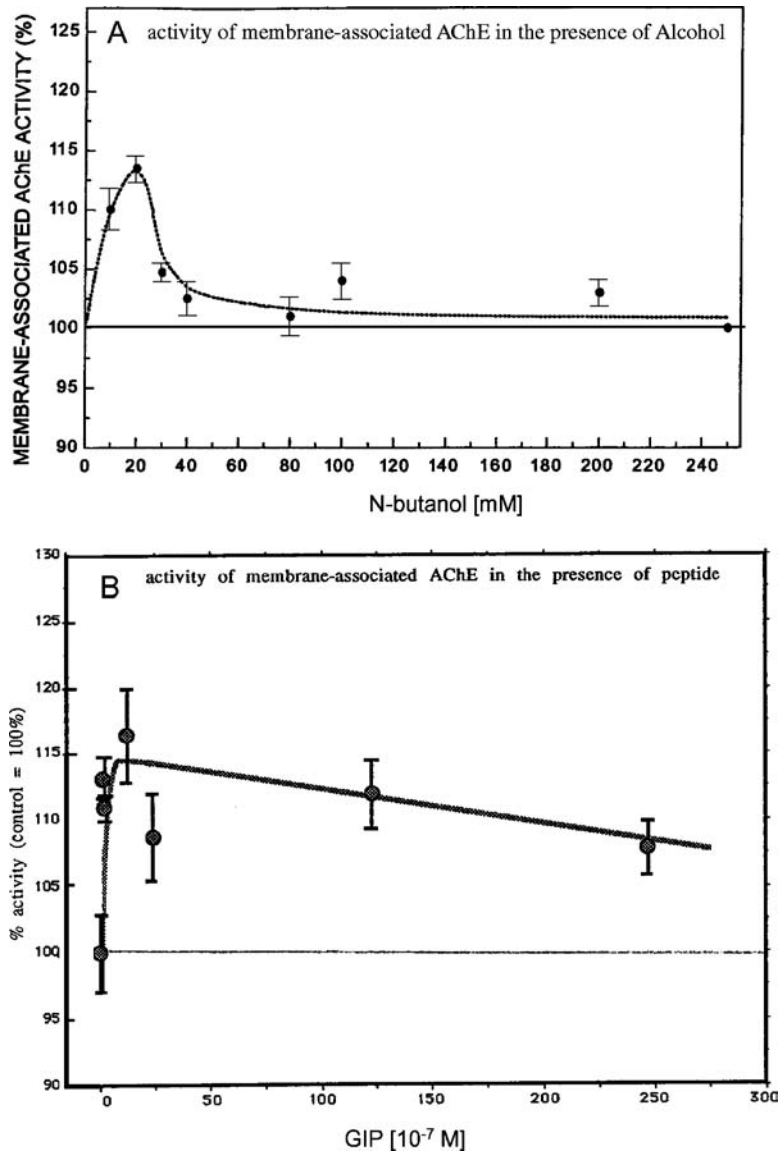

Figure 9. The enzymatic activity of acetylcholinesterase (Ache) in isolated membrane preparations is depicted using either N-butanol (Panel-A) or P149 (Panel-B) as enhancing agents. The Ache-associated membrane vesicles were isolated from Torpedo eel electric organ extracts as described [79]. The effect of P149 on Ache-enriched membranes was an enhancement of enzyme activity greater than that obtained with n-butanol, an established enhancing agent. Note that both alcohol and GIP undergo an initial rise, peaking, and gradual decrease, at increasing concentrations. Control Ache activity was set at 100%. Panel-A is taken from Ref. [79] with permission.

inhibition for several minutes until Epi, which was non-GIP reactive, was added to the incubation bath. Complete platelet aggregation then occurred, achieving nearly 100%. This indicated that Epi employed different Non-GIP reactive cell surface receptors sites for platelet aggregation. Further confirmation of the P149 inhibition of AA-induced aggregation was shown by fluorescent quenching of CD62P platelet surface markers in association with AA-activated platelets.

The secondary step of platelet aggregation liberates AA and initiates its subsequent metabolism. Thromboxane A_2 is produced form AA, causing irreversible platelet aggregation and contraction of vascular bronchial smooth muscle [54]. P149 was a

potent inhibitor of AA-induced platelet aggregation which causes the transformation of cyclo-oxygenases to endoperoxidases. Collagen also induces products of the cyclo-oxygenase pathway but its mode of action does not involve a primary aggregation step. The release of platelet granules is associated with the secondary phase of aggregation. Platelets release four types of granules: (1) α-granules which contain fibrinogen, fibrinectin, and thrombospondin; (2) coagulation-factor granules; (3) dense granules containing serontonin, ATP, ADP, and Ca^{2+} ions; and (4) peroxisomes containing catalase–associated phosphatases. Epinephrine, unlike ADP, does not cause a shape change and does not require the primary aggregation step.

The GIP platelet aggregation inhibition data are listed in Table 6, along with sequence homology to platelet-expressed integrin alpha/beta chains and these chains' specific ECM binding ligands. It was apparent that the full-length P149 showed the greatest inhibitory potencies toward the various activating agents which included collagen, ADP, and AA. However, P149a and P149b also exhibited notable inhibitory capabilities. In contrast, the carboxy-terminal P149c fragment appeared to lack inhibitory capabilities regarding platelet aggregation. It was not surprising that the P149c was devoid of this inhibitory capability, since GenBank identities were not detected in this sequence of GIP, unlike P149a and P149b (Table 3; Table 7).

Tumor-induced platelet aggregation

Tumor cell-induced platelet aggregation is a required step leading to metastasis, as first described by Gasic in the early 1970s [55]. Tumor cells in the vasculature are frequently observed in complexes with platelets, and this association together with the hypercoagulable state of malignant disease, appears to be essential for successful metastasis [55,56]. The ability of tumor cells to induce platelet aggregation is widespread among cancers including breast carcinoma, colon adenocarcinoma, lung carcinoma, melanomas, and others [57]. Platelet participation in the metastatic process is thought to result from a) direct binding of platelets to tumor cells, and (b) the release of soluble activating agents from the tumor cells. These agents would include the classical platelet aggregation activators such as ADP, cathepsin B, thrombin-like proteinases, collagen, and tissue factor-generated thrombin [58]. Thus, platelets act to facilitate all of the intermediate steps of transvascular metastasis including tumor cell retention and arrest, subendothelial interaction, and extravasation from the microvasculature. Blockage at these platelet events could retard or reduce tumor cell metastasis. As noted above, P149 is capable of inhibiting tumor cell adhesion to the ECM and platelet aggregation, both of which are required for successful metastasis.

Previously, a wide array of 30–50 aa peptides derived from true viper and pit viper venoms, termed disintegrins, have been shown to disrupt integrin function and serve as potent inhibitors of platelet aggregation [56]. A disintegrin motif also constitutes a portion of the protein molecules belonging to the ADAM family of metalloproteinases [60], which number among the GenBank matches with P149 in Table 1. The viper-associated disintegrin peptides are hemostasis-disrupting factors that are readily distinguished from the cobra-like venoms, which act as neurotoxins. Similar to P149 (GIP), some disintegrins can produce growth suppression in tumors [61]. Most disintegrins contain the RGD (Arg-Gly-Asp) cell adhesion recognition sequence, are rich in cysteine, and function to block platelet aggregation. Inhibition results from steric blockage of the binding of the GPIIa/IIIb platelet-integrin binding to ECM proteins such as fibrinogen and von Willebrand's factor [62–64]. Since most disintegrins possess the RGD sequence, they are capable of further inhibiting the adhesive functions of other RGD-dependent integrins such as $\alpha_v\beta_5$ (vitronectin receptors) and $\alpha_5\beta_1$, a fibronectin receptor [57,65]. However, by comparison with the integrins, other amino acid adhesion sequences such as Lys-Gly-Asp, may also be operational in the disintegrins. P149 contains the sequence Gly-Glu-Gly (GEG) which is also present in many disintegrins and plays a role in platelet aggregation inhibition (Table 5). Thus, P149, similar to disintegrins, may represent lead molecules for designing novel and potent compounds with clinical value in the inhibition of platelet aggregation and the blockage of the tumor-induced platelet aggregation stage of metastasis. Disintegrins bind to integrins and block their actions, suppressing cancer cell growth and adherence to blood vessel walls and thereby reducing metastasis [60]. Since P149 has been shown to suppress tumor growth and inhibit cell adhesion, it can be proposed that P149 exercises a disintegrin-like action on cancer cell metastasis. Thus, disintegrin-like peptides (i.e. GIP) could constitute a class of chemicals whose

therapeutic potential for metastasis has not yet been fully realized.

Tumor acetylcholinesterases and GIP

Acetylcholinesterases (Ache) are enzymes that hydrolyze the substrate acetylcholine, preventing overstimulation of cholinergic receptors. Although largely localized at cholinergic synaptic sites, cholinesterases such as Ache have been identified in skin, lung, esophagus, liver, placenta and red blood cells, but not in blood plasma [66,67]. Cholinesterases have also been implicated in the process of tumorigenesis, displaying both cholinergic and non-cholinerigic actions, which are associated with mitotic events, cell energy/metabolism, and regulation of divalent cation (Na^{2+}, Ca^{2+}, K^{2+}) transmembrane passage [67–69]. The enzymatic activity of Ache is increased in tumors such as breast, ovarian and bladder cancers, leukemias, glioblastomas, meningiomas, and brain neoplasmas. During tumor growth and progression, Ache genes are amplified and the protein products are abnormally expressed, displaying altered isoforms (variants) and glycosylation patterns [70–72]. Breast cancer epithelia synthesize Ache in the cytoplasmic compartment; Ache is then transported and inserted into the plasma membrane anchored to the glycolipid glycophosphidylinositol [73]. In comparison to normal breast epithelia, breast cancer cells exhibited 1.9 times the Ache enzymatic activity (1.61 and 3.09 mU/mg respectively). Increased cell proliferation, the hallmark of cancer cells, generates mitosis-associated events that further induce overexpression of Ache. Such events can include: (1) estrogen-induced transcription; (2) ER binding to the gene estrogen response element (ERE) (3) muscurinic receptor stimulation of Sp-1 and Egr-1 synthesis; and (4) cytokine stimulation of interleukin-1b production [74–77].

The enzymatic activities of Ache in metastatic foci, in contrast to solid tumors, at first appears to be decreased. Interestingly, the Ache enzymatic activity of breast tumor metastases in auxiliary lymph nodes were 5 times lower in cancerous than in normal lymph nodes tissue [78]. However, the Ache activity in metastatic cell infiltrates was not really significantly different than in the cancer tissues of origin (3.90 and 3.09 mU/mg respectively). Thus, the apparent decrease has been attributed to a "dilution" bystander cell effect. This is because much of the constitutive cell population of the lymph node tissue mass is composed of highly-reactive Ache cells of myeloid lineages (such as β-cells, monocytes, and follicle dendritic cells) which are engaged in immune and inflammatory activities. Ache enzymatic activity is known to be amplified in cells of the erythroid and myeloid series, many of which populate the lymph nodes [77,78]. Thus, the Ache activity in metastatic cancer cells give the appearance of decreased activity which is really not the case. Furthermore, Ache oligomeric forms from metastatic cells are composed only of monomers and dimers, while the Ache in normal lymph nodes include additional tetrameric and asymmetric forms [71,78]. Overall, it was determined that both the content and composition of Ache systems (i.e., nicotinic/muscurinic receptors, choline acetyltransferase, and Ache forms) were profoundly altered after invasion of lymph nodes by neoplastic cells.

In a corollary model to the cholinesterase presence in cancers cells, the enzymatic activities of Ache was determined in the presence of GIP using non-cancer isolated membrane preparations of Ache. The Ache associated-membrane preparations were derived from the electric organ of Torpedo eel extracts [79]. The activities of Ache were determined in acetylcholine receptor-enriched eel membrane vesicles as previously described [80]. Since Ache is synthesized in breast cell cytoplasm and undergoes plasma membrane insertion, Ache electric organ membrane vesicle preparations can provide a model of isolated Ache membrane activity in response to P149. In the studies using the torpedo eel membrane vesicles, it was demonstrated that Ache membrane activity was significantly enhanced with P149 present in the reaction vessel. The GIP effect on Ache membrane vesicle activity was titratable over a series of concentration points with peak enhancement at 10×10^{-7} M (Figure 9). Control solutions consisted of compounds of organic alcohols (i.e. N-butanol) which are known to influence Ache activity. Moreover, P149 was found to be as potent an enhancing agent than was N-butanol under comparable experimental conditions. It can be proposed that P149 either (1) promotes Ache activities directly, (2) binds to Ache substrates; or (3) neutralizes non-specific and/or other broad-spectrum esterases that compete with Ache. In this regard, P149 has also been demonstrated to affect esterase activity in the postnatal rat uterus (Table 7) [6]. The P149-enhanced membrane activity of Ache indicated possible involvement of GIP with the membrane (vesicle) lipid bilayer itself. This can be deduced

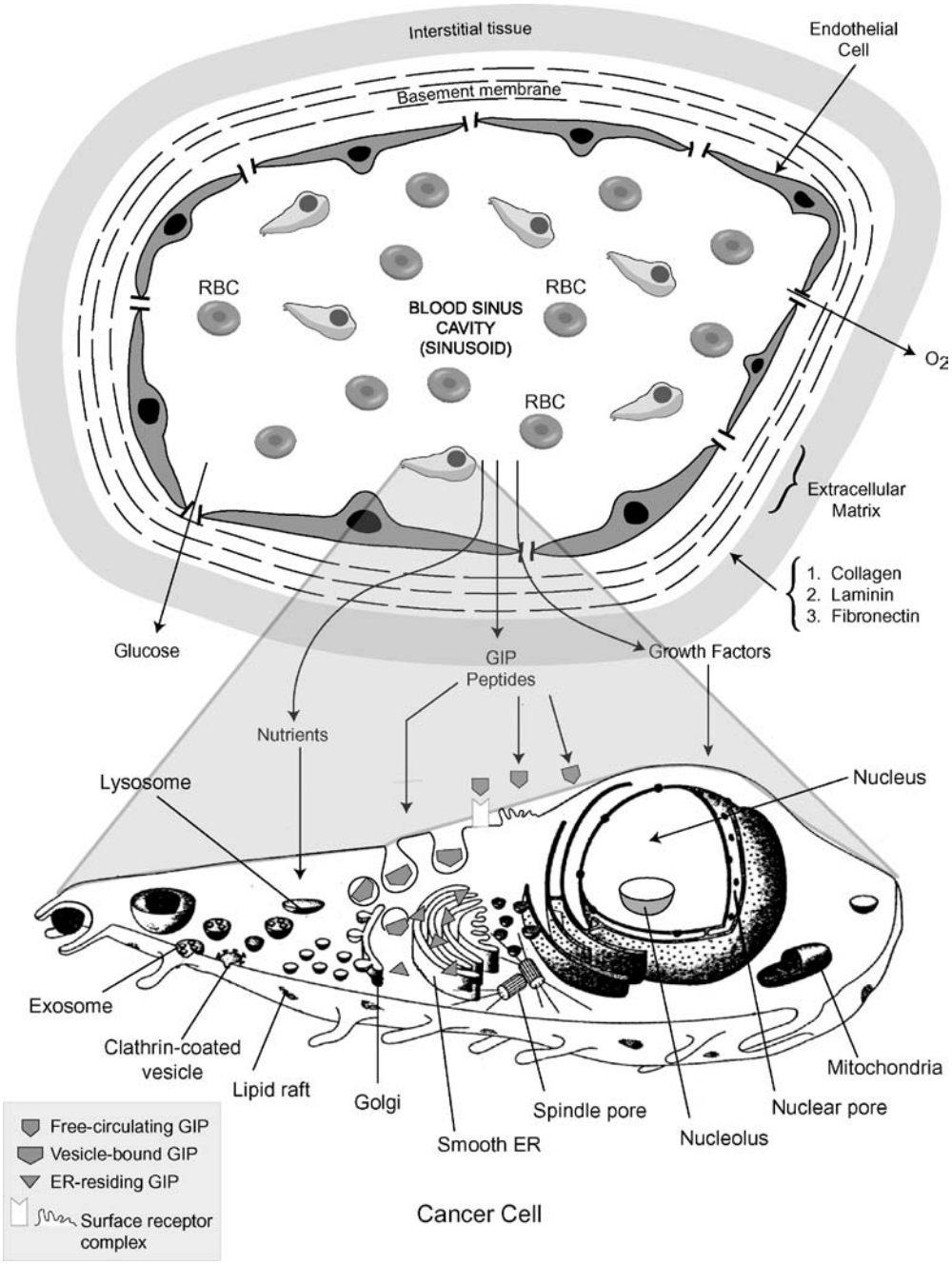

Figure 10. The mechanism of decoy ligand endocytosis of the Growth Inhibitory peptide (GIP) is depicted. Metastatic cancer cells from a blood sinus (top half of picture) exit through intraendothelial gaps to surrounding tissues. Free circulating GIP binds to an unknown cancer cell receptor (G-coupled?) and is endocytosed but does not activate the receptor to transduce a signal to the cell interior. A cut-away view of the epithelial metastatic cell is shown. Labels indicate tumor cell organelles. Note that the GIP is targeted to the smooth endoplasmic reticulum (ER) surrounding the nucleus (perinuclear location) as described in Ref. [18].

from findings of previous studies [79,80] which showed that action of the higher alcohols (i.e. n-butanols) increased the membrane fluidity of the membrane vesicles; thus, lipid solubility and molecular size were deemed to be factors important for the alcohols to insert into the membrane lipid domains [80]. The observation that the vesicle Ache activity was enhanced by P149 again confirmed that GIP is indeed highly reactive at membrane interfaces; that is, it is a membrane-reactive agent.

Concluding statements

It is evident from the present review, that the AFP-derived GIP (P149) is a major participant in tumor cell surface interactions. Clearly, GIP is a capable suppressor of tumor proliferation in both rodent and human cancer models. It was also shown that GIP's biological activity is dependent on its oligomeric state, specifically its trimer (linear) as compared to monomer (cyclic) configuration. In studies using a cell adhesion assay, it was demonstrated that P149 inhibited tumor cell adhesion against a variety of ECM proteins, many of which serve as basement membrane and clotting constituents. P149-coated coverslips were also employed to show that tumor cell attachment, migration, and spreading were negatively influenced by AFP peptides. In assays using activated platelet suspensions, P149 was shown capable of blocking all phases of platelet aggregation against a variety of agonists. Finally, the use of isolated membrane preparations possessing Ache as a reporter enzyme showed that GIP was an active participant at membrane vesicle interfaces. Overall, the inhibition by P149 of cell surface activities such as tumor cell adhesion, migration, and platelet-binding would serve to seriously impair the ability of tumor cells to spread and metastaze.

Although the mechanism of GIP's tumor growth suppression has been proposed as receptor blockage of G-protein linked signal transduction, the precise mode of action has yet to be fully elucidated (Figure 10). The suppressive mechanism of action of GIP must be at a level common to a variety of cell types since nine types of tumor cells were growth-suppressed (Table 5). Previous studies have also shown that the growth inhibitory property of P149 crosses species barriers and is observed in amphibians, birds, and mammals including man and rodents (Table 7). These observations suggest an inhibitory mechanism of action of P149 that is common to many different kinds of animal cells [81]. These shared events of GIP's action appears to occur primarily as cell surface activities being representative of cell adhesion, migration, aggregation, agglutination, cytoskeletal-mediatated cell shape and form, and endocytosis. Such conserved actions indicate that GIP appears to be a plasma membrane-active agent that can interrupt or disable integrin-associated and platelet dependent physiological actions on tumor growth, progression, and metastasis.

Acknowledgment

We thank Dr. James Dias, Dr. Charles Hauer, Dr. Robert MacColl, Dr. Li-Ming Changchien, and Leslie Eisele of the Core Facilities of the Wadsworth Center for their expert preparations, characterization, purification, and various biological and biochemical analyses of the peptides. Gratitude is also expressed to Doris Collins, MD, New York State-certified pathologist, for her histological evaluation of the H&E stained mouse tissue sections. The cell culture technical assistance of Dr. Gisela Caceres, Rumbaugh Goodwin Institute, is gratefully acknowledged. The student technical assistance of Adam Bulakowski and Erin Volk are also appreciated. Finally, the author wishes to express his sincerest thanks and gratitude to the manuscript co-authors for their assistance and to Lynda M. Jury for her commitment and time expenditure in the excellent typing and processing of the manuscript, references, and tables of this report.

References

1. Ingham KC, Brew SA, Erickson HP: Localization of a cryptic binding site for tenascin on fibronectin. J Biol Chem 279: 28132–28135, 2004
2. Podolnikova NP, Yakubenko VP, Volkov GL, Plow EF, Ugarova TP: Identification of a novel binding site for platelet integrins alpha IIb beta 3 (GPIIbIIIa) and alpha 5 beta 1 in the gamma C-domain of fibrinogen. J Biol Chem 278: 32251–32258, 2003
3. Mizejewski G. New insights into AFP structure and function: Potential biomedical applications. Alpha-fetoprotein and Congenital Disorders, ed. Mizejewski G, Porter IH, Orlando, Academic Press, 1985, pp. 5–34.
4. Mizejewski GJ: Alpha-fetoprotein as a biologic response modifier: Relevance to domain and subdomain structure. Proc Soc Exp Biol Med 215: 333–362, 1997

5. Mizejewski GJ: Alpha-fetoprotein structure and function: relevance to isoforms, epitopes, and conformational variants. Exp Biol Med (Maywood) 226: 377–408, 2001
6. Mizejewski GJ, Dias JA, Hauer CR, Henrikson KP, Gierthy J: Alpha-fetoprotein derived synthetic peptides: assay of an estrogen-modifying regulatory segment. Mol Cell Endocrinol 118: 15–23, 1996
7. Gershwin ME, Castles JJ, Makishima R: Accelerated plasmacytoma formation in mice treated with alpha-fetoprotein. J Natl Cancer Inst 64: 145–149, 1980
8. Uriel J: The physiological role of alpha-fetoprotein in cell growth and differentiation. J Nucl Med Allied Sci 33: 12–17, 1989
9. Wang XW, Xu B: Stimulation of tumor-cell growth by alpha-fetoprotein. Int J Cancer 75: 596–599, 1998
10. Li MS, Li PF, Yang FY, He SP, Du GG, Li G: The intracellular mechanism of alpha-fetoprotein promoting the proliferation of NIH 3T3 cells. Cell Res 12: 151–156, 2002
11. Liang OD, Korff T, Eckhardt J, Rifaat J, Baal N, Herr F, Preissner KT, Zygmunt M: Oncodevelopmental alpha-fetoprotein acts as a selective proangiogenic factor on endothelial cell from the fetomaternal unit. J Clin Endocrinol Metab 89: 1415–1422, 2004
12. Takahashi Y, Ohta T, Mai M: Angiogenesis of AFP producing gastric carcinoma: correlation with frequent liver metastasis and its inhibition by anti-AFP antibody. Oncol Rep 11: 809–813, 2004
13. Li MS, Li PF, Chen Q, Du GG, Li G: Alpha-fetoprotein stimulated the expression of some oncogenes in human hepatocellular carcinoma Bel 7402 cells. World J Gastroenterol 10: 819–824, 2004
14. Um SH, Mulhall C, Alisa A, Ives AR, Karani J, Williams R, Bertoletti A, Behboudi S: Alpha-fetoprotein impairs APC function and induces their apoptosis. J Immunol 173: 1772–1778, 2004
15. Vakharia D, Mizejewski GJ: Human alpha-fetoprotein peptides bind estrogen receptor and estradiol, and suppress breast cancer. Breast Cancer Res Treat 63: 41–52, 2000
16. Sinenko SA, Belyaev NN, Mizejewski G: Analysis of functional activities of human alpha-fetoprotein with new monoclonal antibodies and a synthetic peptide. Tumor Biol 21: 112, 2000
17. Kuznetsova IM, Turoverov KK, Uversky VN: Use of the phase diagram method to analyze the protein unfolding-refolding reactions: Fishing out the "invisible" intermediates. J Proteome Res 3: 485–494, 2004
18. Mizejewski GJ, MacColl R: Alpha-fetoprotein growth inhibitory peptides: Potential leads for cancer therapeutics. Mol Cancer Ther 2: 1243–1255, 2003
19. Mizejewski G, Smith G, Butterstein G: Review and Proposed Action of alpha-fetoprotein growth inhibiting peptides as estrogen and cytoskeletal-associated factors. Intl Journal Cell Biology 28: 913–933, 2004.
20. Czokalo M, Tomasiak M: Alpha fetoprotein inhibits aggregation of human platelets. Haematologia (Budap) 22: 11–18, 1989
21. Mizejewski GJ: Levels of alpha-fetoprotein during pregnancy and early infancy in normal and disease states. Obstet Gynecol Surv 58: 804–826, 2003
22. Brenner T, Stupp-Da-Costa Y, Sicsic C, Abramsky O: Inhibition by alpha-fetoprotein fractions of hemagglutination reactions between A and B antigens of human red blood cells and specific antisera. Clin Immunol Immunopathol 34: 20–26, 1985
23. Dauphinee MJ, Mizejewski GJ: Human alpha-fetoprotein contains potential heterodimerization motifs capable of interaction with nuclear receptors and transcription/growth factors. Med Hypotheses 58: 453–461, 2002
24. Eisele LE, Mesfin FB, Bennett JA, Andersen TT, Jacobson HI, Soldwedel H, MacColl R, Mizejewski GJ: Studies on a growth-inhibitory peptide derived from alpha-fetoprotein and some analogs. J Pept Res 57: 29–38, 2001
25. Eisele LE, Mesfin FB, Bennett JA, Andersen TT, Jacobson HI, Vakharia DD, MacColl R, Mizejewski GJ: Studies on analogs of a peptide derived from alpha-fetoprotein having antigrowth properties. J Pept Res 57: 539–546, 2001.
26. MacColl R, Eisele LE, Stack RF, Hauer C, Vakharia DD, Benno A, Kelly WC, Mizejewski GJ: Interrelationships among biological activity, disulfide bonds, secondary structure, and metal ion binding for a chemically synthesized 34-amino-acid peptide derived from alpha-fetoprotein. Biochim Biophys Acta 2 1528: 127–134, 2001
27. Butterstein G, MacColl R, Mizejewski GJ, Eisele LE, Meservey M: Biophysical studies and anti-growth activities of a peptide, a certain analog and a fragment peptide derived from alpha-fetoprotein. J Pept Res 61: 213–218, 2003
28. Butterstein G, Morrison J, Mizejewski GJ: Effect of alpha-fetoprotein and derived peptides on insulin- and estrogen-induced fetotoxicity. Fetal Diagn Ther 18: 360–369, 2003
29. Mizejewski GJ: An apparent dimerization motif in the third domain of alpha-fetoprotein: Molecular mimicry of the steroid/thyroid nuclear receptor superfamily. Bioessays 15: 427–432, 1993
30. Mizejewski GJ: Role of integrins in cancer: Survey of expression patterns. Proc Soc Exp Biol Med 222: 124–138, 1999
31. Murawaki Y, Yamamoto H, Kawasaki H, Shima H: Serum tissue inhibitor of metalloproteinases in patients

with chronic liver disease and with hepatocellular carcinoma. Clin Chim Acta 218: 47–58, 1993
32. Parsons DF, Foley J, Marko M, Wansor K: Immediate ascites conversion of mammary tumors induced in NYLR/Nya mice by 7,12-dimethylbenz-[a] anthracene and urethane feeding and by forced breeding. Cancer Invest 4: 109–126, 1986
33. Hurst J, Maniar N, Tombarkiewicz J, Lucas F, Roberson C, Steplewski Z, James W, Perras J: A novel model of a metastatic human breast tumour xenograft line. Br J Cancer 68: 274–276, 1993
34. Morrissey JJ, Raney S: A metastatic breast tumor cell line, GI-101A, is estrogen receptorpositive and responsive to estrogen but resistant to tamoxifen. Cell Biol Int 22: 413–419, 1998
35. Garewal HS, Ahmann FR, Schifman RB, Celniker A: ATP assay: Ability to distinguish cytostatic from cytocidal anticancer drug effects. J Natl Cancer Inst 77: 1039–1045, 1986
36. Kuzmits R, Rumpold H, Muller MM, Schopf G: The use of bioluminescence to evaluate the influence of chemotherapeutic drugs on ATP-levels of malignant cell lines. J Clin Chem Clin Biochem 24: 293–298, 1986
37. Kurbacher CM, Cree IA, Bruckner HW, Brenne U, Kurbacher JA, Muller K, Ackermann T, Gilster TJ, Wilhelm LM, Engel H, Mallmann PK, Andreotti PE: Use of an *ex vivo* ATP luminescence assay to direct chemotherapy for recurrent ovarian cancer. Anticancer Drugs 9: 51–57, 1998
38. Ginsberg MH, Loftus JC, D'Souza S, Plow EF: Ligand binding to integrins: common and ligand specific recognition mechanisms. Cell Differ Dev 32: 203–213, 1990
39. Hynes RO: Integrins: versatility, modulation, and signaling in cell adhesion. Cell 69: 11–25, 1992
40. Ruoslahti E: Control of cell motility and tumor invasion by extracellular matrix interactions. Br J Cancer 66: 239–242, 1992
41. Gui GP, Puddefoot JR, Vinson GP, Wells CA, Carpenter R: In vitro regulation of human breast cancer cell adhesion and invasion via integrin receptors to the extracellular matrix. Br J Surg 82: 1192–1196, 1995
42. Juliano RL: The role of beta 1 integrins in tumors. Semin Cancer Biol 4: 277–283, 1993.
43. Ruoslahti E: Stretching is good for a cell. Science 276: 1345–1346, 1997
44. Dedhar S: Integrin mediated signal transduction in oncogenesis: an overview. Cancer Metastasis Rev 14: 165–172, 1995
45. Liu Z, Brattain MG, Appert H: Differential display of reticulocalbin in the highly invasive cell line, MDA-MB-435, versus the poorly invasive cell line, MCF-7. Biochem Biophys Res Commun 231: 283–289, 1997
46. Burridge K, Chrzanowska-Wodnicka M: Focal adhesions, contractility, and signaling. Annu Rev Cell Dev Biol 12: 463–518, 1996
47. Virtanen I, Korhonen M, Kariniemi AL, Gould VE, Laitinen L, Ylanne J: Integrins in human cells and tumors. Cell Differ Dev 32: 215–227, 1990.
48. Edwards JG, Hameed H, Campbell G: Induction of fibroblast spreading by Mn2+: A possible role for unusual binding sites for divalent cations in receptors for proteins containing Arg-Gly-Asp. J Cell Sci 89: 507–513, 1988
49. Kinlough-Rathbone RL, Packham MA, Mustard JF, Platelet Aggregation in Measurements of Platelet Function, ed. Harker LA,Zimmerman TS., Churchill Livingstone, London, 1983, pp. 64–87
50. Whittle BJR, Hamid S, Lidbury P, Rosam AC, Specificity between the anti-aggregatory actions of prostacyclin, prostaglandin E1 and D2 on platelets in. Mechanisms of stimulus-response coupling in platelets, ed. V.V. K, MacIntyre DE, Scully MF. New York and London, Plenum Press 1985, pp. 109–115
51. Hamberg M, Svensson J, Samuelsson B: Thromboxanes: a new group of biologically active compounds derived from prostaglandin endoperoxides. Proc Natl Acad Sci USA 72: 2994–2998, 1975
52. Chen CS, Mrksich M, Huang S, Whitesides GM, Ingber DE: Geometric control of cell life and death. Science 276: 1425–1428, 1997
53. Fox JE, Reynolds CC, Boyles JK: Studying the platelet cytoskeleton in Triton X-100 lysates. Methods Enzymol 215: 42–58, 1992
54. Ellis EF, Oelz O, Roberts LJ, 2nd, Payne NA, Sweetman BJ, Nies AS, Oates JA: Coronary arterial smooth muscle contraction by a substance released from platelets: evidence that it is thromboxane A2. Science 193: 1135–1137, 1976
55. Gasic GJ, Gasic TB, Galanti N, Johnson T, Murphy S: Platelet-tumor-cell interactions in mice. The role of platelets in the spread of malignant disease. Int J Cancer 11: 704–718, 1973
56. Gould RJ, Polokoff MA, Friedman PA, Huang TF, Holt JC, Cook JJ, Niewiarowski S: Disintegrins: A family of integrin inhibitory proteins from viper venoms. Proc Soc Exp Biol Med 195: 168–171, 1990
57. Sheu JR, Lin CH, Peng HC, Huang TF: Triflavin, an Arg-Gly-Asp-containing peptide, inhibits the adhesion of tumor cells to matrix proteins via binding to multiple integrin receptors expressed on human hepatoma cells. Proc Soc Exp Biol Med 213: 71–79, 1996
58. Sheu JB, Ko WC, Hung WC, Peng HC, Huang TF: Interaction of thrombin-activated platelets with extracellular matrices (fibronectin and vitronectin): comparison of the activity of Arg-Gly-Asp-containing venom peptides and monoclonal antibodies against glycoprotein IIb/IIIa complex. J Pharm Pharmacol 49: 78–84, 1997

59. Scarborough RM, Rose JW, Hsu MA, Phillips DR, Fried VA, Campbell AM, Nannizzi L, Charo IF: Barbourin. A GPIIb-IIIa-specific integrin antagonist from the venom of Sistrurus m. barbouri. J Biol Chem 266: 9359–9362, 1991
60. Chiang HS, Swaim MW, Huang TF: Characterization of platelet aggregation induced by human colon adenocarcinoma cells and its inhibition by snake venom peptides, trigramin and rhodostomin. Br J Haematol 87: 325–331, 1994
61. Nierodzik ML, Klepfish A, Karpatkin S: Role of platelet integrin GPIIb-GPIIIa, fibronectin, von Willebrand factor, and thrombin in platelet-tumor interaction *in vitro* and metastasis *in vivo*. Semin Hematol 31: 278–288, 1994.
62. Wolfsberg TG, Primakoff P, Myles DG, White JM: ADAM, a novel family of membrane proteins containing A Disintegrin And Metalloprotease domain: multipotential functions in cell-cell and cell-matrix interactions. J Cell Biol 131: 275–278, 1995
63. Chiang HS, Swaim MW, Huang TF: Characterization of platelet aggregation induced by human breast carcinoma and its inhibition by snake venom peptides, trigramin and rhodostomin. Breast Cancer Res Treat 33: 225–235, 1995
64. Coller BS, Anderson KM, Weisman HF: The anti-GPIIb-IIIa agents: fundamental and clinical aspects. Haemostasis 26: 285–293, 1996
65. Nurden AT: New thoughts on strategies for modulating platelet function through the inhibition of surface receptors. Haemostasis 26: 78–88, 1996
66. Ruiz-Espejo F, Cabezas-Herrera J, Illana J, Campoy FJ, Vidal CJ: Cholinesterase activity and acetylcholinesterase glycosylation are altered in human breast cancer. Breast Cancer Res Treat 72: 11–22, 2002
67. Sastry BV: Human placental cholinergic system. Biochem Pharmacol 53: 1577–1586, 1997
68. Greenfield SA, Jack JJ, Last AT, French M: An electrophysiological action of acetylcholinesterase independent of its catalytic site. Exp Brain Res 70: 441–444, 1988
69. Greenfield SA: A noncholinergic action of acetylcholinesterase (AChE) in the brain: from neuronal secretion to the generation of movement. Cell Mol Neurobiol 11: 55–77, 1991
70. Nitsch RM, Rossner S, Albrecht C, Mayhaus M, Enderich J, Schliebs R, Wegner M, Arendt T, von der Kammer H: Muscarinic acetylcholine receptors activate the acetylcholinesterase gene promoter. J Physiol Paris 92: 257–264, 1998
71. Fernandez HL, Moreno RD, Inestrosa NC: Tetrameric (G4) acetylcholinesterase: structure, localization, and physiological regulation. J Neurochem 66: 1335–1346, 1996
72. Grisaru D, Sternfeld M, Eldor A, Glick D, Soreq H: Structural roles of acetylcholinesterase variants in biology and pathology. Eur J Biochem 264: 672–686, 1999
73. Massoulie J: The origin of the molecular diversity and functional anchoring of cholinesterases. Neurosignals 11: 130–143, 2002
74. Li Y, Liu L, Kang J, Sheng JG, Barger SW, Mrak RE, Griffin WS: Neuronal-glial interactions mediated by interleukin-1 enhance neuronal acetylcholinesterase activity and mRNA expression. J Neurosci 20: 149–155, 2000
75. Speirs V, Kerin MJ, Newton CJ, Walton DS, Green AR, Desai SB, Atkin SL: Evidence for transcriptional activation of ERalpha by IL-1beta in breast cancer cells. Int J Oncol 15: 1251–1254, 1999
76. Layer PG, Willbold E: Novel functions of cholinesterases in development, physiology and disease. Prog Histochem Cytochem 29: 1–94, 1995
77. Lampert IA, Van Noorden S: Acetyl cholinesterase is expressed in the follicular dendritic cells of germinal centres: Differences between normal and neoplastic follicles. J Pathol 180: 169–174, 1996
78. Ruiz-Espejo F, Cabezas-Herrera J, Illana J, Campoy FJ, Munoz-Delgado E, Vidal CJ: Breast cancer metastasis alters acetylcholinesterase activity and the composition of enzyme forms in axillary lymph nodes. Breast Cancer Res Treat 80: 105–114, 2003
79. Wang Y, Chen CH: Acetylcholine receptor-enriched membrane vesicles in response to ethanol: Activity and microcalorimetric studies. Biophys Chem 43: 51–59, 1992
80. Lasner M, Roth LG, Chen CH: Structure-functional effects of a series of alcohols on acetylcholinesterase-associated membrane vesicles: Elucidation of factors contributing to the alcohol action. Arch Biochem Biophys 317: 391–396, 1995
81. Butterstein GM, Mizejewski GJ: Alpha-fetoprotein inhibits frog metamorphosis: Implications for protein motif conservation. Comp Biochem Physiol A Mol Integr Physiol 124: 39–45, 1999